ACS Chemical Neuroscience

pubs.acs.org/chemneuro Research Article

Oxidation of Dueling Cysteine Promotes Subunit Exchange in SOD1

Ao Yun Zhang,[§] Chad M. Dashnaw,[§] Mayte Gonzalez, Jordan C. Koone, Nick A. Wells, Colin A. Smith, Matthew J. Guberman-Pfeffer, and Bryan F. Shaw*

Cite This: *ACS Chem. Neurosci.* 2023, 14, 1547−1560 Read Online

ACCESS | Metrics & More | Article Recommendations | Supporting Information

ABSTRACT: The heterodimerization of wild-type (WT) Cu, Zn superoxide dismutase-1 (SOD1) and mutant SOD1 might be a critical step in the pathogenesis of SOD1-linked amyotrophic lateral sclerosis (ALS). Post-translational modifications that accelerate SOD1 heterodimerization remain unidentified. Here, we used capillary electrophoresis to quantify the effect of cysteine-111 oxidation on the rate and free energy of ALS mutant/WT SOD1 heterodimerization. The oxidation of Cys_{111}-β-SH to sulfinic and sulfonic acid (by hydrogen peroxide) increased rates of heterodimerization (with unoxidized protein) by ∼3-fold. Cysteine oxidation drove the equilibrium free energy of SOD1 heterodimerization by up to $\Delta\Delta G = -5.11 \pm 0.36$ kJ mol^{-1}. Molecular dynamics simulations suggested that this enhanced heterodimerization, between oxidized homodimers and unoxidized homodimers, was promoted by electrostatic repulsion between the two "dueling" Cys_{111}-SO_2^-/SO_3^-, which point toward one another in the homodimeric state. Together, these results suggest that oxidation of Cys-111 promotes subunit exchange between oxidized homodimers and unoxidized homodimers, regardless of whether they are mutant or WT dimers.

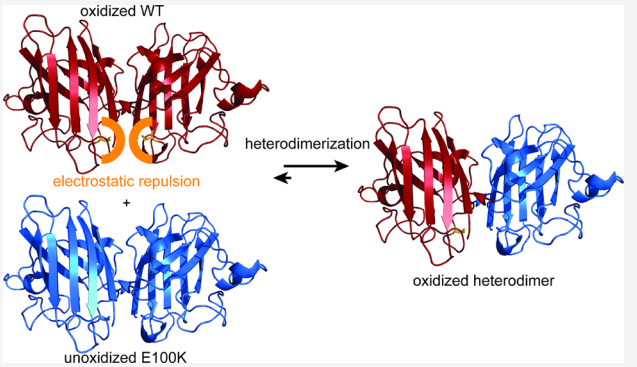

KEYWORDS: *protein aggregation, amyloid, oxidative stress, reactive oxygen species, motor neuron, capillary electrophoresis, sulfenic, sulfinic, sulfonic acid*

INTRODUCTION

Nearly 200 different mutations—largely heterozygous missense mutations—in the superoxide dismutase gene (SOD1) cause ∼2% of amyotrophic lateral sclerosis (ALS).[1−4] Survival times for people with SOD1-linked ALS vary by decades per SOD1 mutation.[5−7] For example, the A4V missense mutation presents with a survival time of 1.4 ± 0.7 years after diagnosis,[8] whereas survival times for the H46R mutation are ∼17 years.[9] This range is uncommon for monogenic neurodegenerative disorders that typically present with wider variation in onset age and smaller variation in survival time per mutation.[10−14]

This clinical variation still perplexes biochemical researchers, in part because it cannot be explained by the biophysical properties of misfolded or native SOD1 (rate and free energy of folding, dimerization, and misfolding; electrostatic charge; affinity for Cu/Zn (either singularly or collectively)).[2,5,6,15,16] However, most failed correlations have ignored the wild-type (WT) SOD1 protein, which can heterodimerize with mutant SOD1.[2,17] We hypothesize that native or non-native interactions between wild-type and mutant SOD1 might fill a few gaps in our biophysical-chemical understanding of the clinical diversity of this monogenic disorder.

The mutant/wild-type heterodimer has not been characterized as well as homodimeric counterparts.[2,17] *In vitro*, the subunits of homodimeric mutant SOD1 and homodimeric WT SOD1 exchange on a time scale of minutes to days depending upon metalation state: $t_{1/2} \approx 0.3-0.5$ h for apo states and $t_{1/2} \approx 3-13$ h for metalated states.[17] However, mutant/WT SOD1 heterodimerization is only marginally favorable at equilibrium, with free energies of heterodimerization (ΔG_{Het}) varying from −0.73 to −3.05 kJ mol^{-1} according to capillary electrophoresis.[17]

In vivo, the heterodimerization of mutant/WT SOD1 appears to somehow promote the aggregation and neurotoxicity of mutant SOD1.[18−21] In transgenic mice expressing ALS mutant SOD1, the coexpression of the WT SOD1 protein can accelerate disease progression.[19,22] In one particular case, the A4V SOD1 mouse, the coexpression of WT SOD1 is required for disease onset.[22] The mechanism by which WT SOD1 triggers ALS in the A4V SOD1 transgenic mouse or simply enhances symptoms of ALS in other mutant SOD1 mice is unknown[18,23] but could involve: (i) direct interactions

Received: March 17, 2023
Accepted: March 24, 2023
Published: April 6, 2023

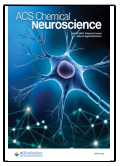

with mutant SOD1 and (ii) indirect mechanisms, including competition for protective factors such as chaperones or $Cu^{1+/2+}$ and Zn^{2+} ions.[23,24]

A previous study of five ALS mutant SOD1 proteins—including three "cryptic" mutants whose $\Delta G_{folding}$ and thermostability are not significantly different from WT SOD1—found that the measured ΔG_{Het} weakly correlated with patient survival time by ∼ +5 years per kJ. Notably, the clinically severe D101N protein, whose survival is as short as the A4V protein (∼2 years), exhibited the most favorable ΔG_{Het}.[17] This favorable ΔG_{Het} is the only biophysical property that we can find for the cryptic D101N SOD1 that might explain why such a thermostable, "wild-type like" protein exhibits the same clinical severity as the highly unstable A4V SOD1 protein (which is intrinsically disordered in its nascent state[25]).

The chemical biology surrounding mutant/WT SOD1 heterodimerization has remained enigmatic because heterodimers are difficult to isolate from preceding homodimers.[26] The SOD1 protein—a long-lived protein—acquires myriad post-translational modifications during its lifetime (functional and detrimental)[27] including: glutathionlylation of free cysteine,[28] lysine acetylation,[29,30] asparagine deamidation,[31] oxidation of histidine,[32] tryptophan,[33] and cysteine,[34,35] phosphorylation,[36] and palmitoylation.[37] The effect of any of these modifications on rates or ΔG of heterodimerization remain unknown. Oxidation of free cysteine in SOD1 is of particular interest as SOD1 produces and interacts with H_2O_2 (a known oxidant involved in redox signaling).[38,39]

This study used capillary electrophoresis (CE) to quantify the effect of cysteine-111 oxidation on the rate and ΔG_{Het} of heterodimerization of ALS mutant and WT SOD1. The SOD1 monomer contains two free cysteines: C6 and C111. Cysteine-111 is solvent exposed (Figure 1), reactive, and a therapeutic target in SOD1-linked ALS.[40,41] Cysteine-111 can undergo selective oxidation to form sulfenic (R-SOH), sulfinic (R-SO_2^-), and sulfonic (R-SO_3^-) acids.[34,42−44] In general, the oxidation of cysteine plays a functional role in redox signaling.[45−48] The SOD1 enzyme is predisposed to cysteine oxidation, *per se*, as both reactants and products of SOD1 catalysis ($O_2^{\bullet-}$, O_2, and H_2O_2) can oxidize cysteine.[35,49] Cysteine-111 oxidation in SOD1 has been hypothesized to play a role in ALS by accelerating certain types of SOD1 aggregation or altering proteostasis.[34,35,50,51] Regardless of the role of oxidative stress in SOD1-linked ALS, we are interested (in this paper) in simply determining how C111 oxidation affects the rate and ΔG_{Het} of WT/mutant heterodimerization.

RESULTS AND DISCUSSION

This study examined the heterodimerization of the ALS-linked E100K variant of SOD1 with oxidized forms of WT SOD1. The principal tool used to measure the rate and ΔG_{Het} of heterodimerization, capillary electrophoresis, separates proteins based upon their net charge and hydrodynamic drag in a bare fused-silica capillary. CE is one of the only tools capable of rapidly and accurately measuring the heterodimerization of these two proteins.[24]

We focused on the E100K mutation because it can be separated from the WT SOD1 at a higher resolution than other ALS mutants that we have studied with CE (isoelectric variants cannot be separated).[52] While the E100K substitution alters the formal net negative charge of each subunit by two units, prior studies with "protein charge ladders" show that the substitution alters the actual net charge of folded solvated SOD1 by +1.89 ± 0.04 units per subunit at pH 7.4.[52]

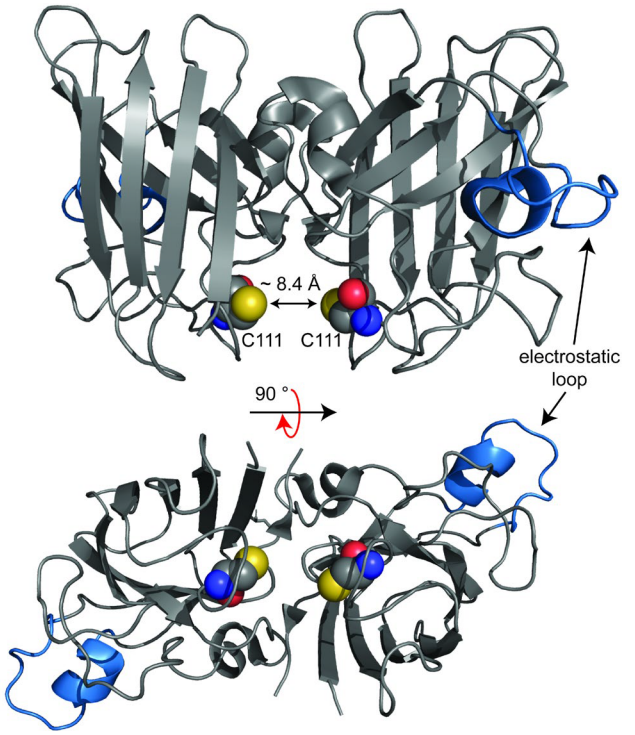

Figure 1. Structure of homodimeric wild-type SOD1 (PDB: 1HL5) with C111 shown with spheres. Cysteine-111 of each subunit is solvent exposed and separated by ∼8.4 Å. The electrostatic loop is highlighted in blue.

Oxidation of Cys-111 in WT SOD1. Cysteine-oxidized WT SOD1 was prepared in potassium phosphate buffer (pH 7.4) by incubation of SOD1 (∼100 μM SOD1 dimer) with 25 mM hydrogen peroxide over 48 h at 23 °C. Oxidation shifted the electropherogram peak by ∼1 mobility unit (Figure 2A). This reaction resulted in near complete oxidation of SOD1, i.e., addition of two and three oxygen atoms per monomer (Figure 2B). Integration of mass spectra demonstrated that 25% of WT SOD1 possessed three oxygens; 66% possessed two oxygens; 7% possessed one oxygen; and 2% was unoxidized (Figure 2B; the molecular weight of unoxidized SOD1 is ∼15844 Da per monomer). Trypsinization and LC−MS/MS of oxidized WT SOD1 protein identified C111 as the site of oxidation (Figure 2E), with oxidation found at no other residues (His, Cys, or Trp). The masses of modifications at C111 are 32 and 48 Da, consistent with R-SO_2^- and R-SO_3^-. SOD1 was oxidized in the apo state to avoid off target oxidation (of histidine). For example, studies have shown that oxidation of metalated SOD1 in hydrogen peroxide results in the oxidation of metal coordinated histidine residues and the release of metal ions.[53−55] In the apo state, however, cysteine residues appear to be the primary target of oxidation.[51,56]

The effect of C111 oxidation on the structure of WT apo-SOD1 was assessed with amide H/D exchange and mass spectrometry (Figure 2C,D). Amide H/D exchange was measured from 2 to 60 min. Across these time scales, the rates of global amide H/D exchange are similar in oxidized WT SOD1 and unoxidized WT SOD1 (Figure 2C,D). This similarity suggests that Cys_{111}-β-SH oxidation to Cys_{111}-SO_2^- to Cys_{111}-SO_3^- does not disrupt the hydrophobic core of WT

https://doi.org/10.1021/acschemneuro.3c00174
ACS Chem. Neurosci. 2023, 14, 1547−1560

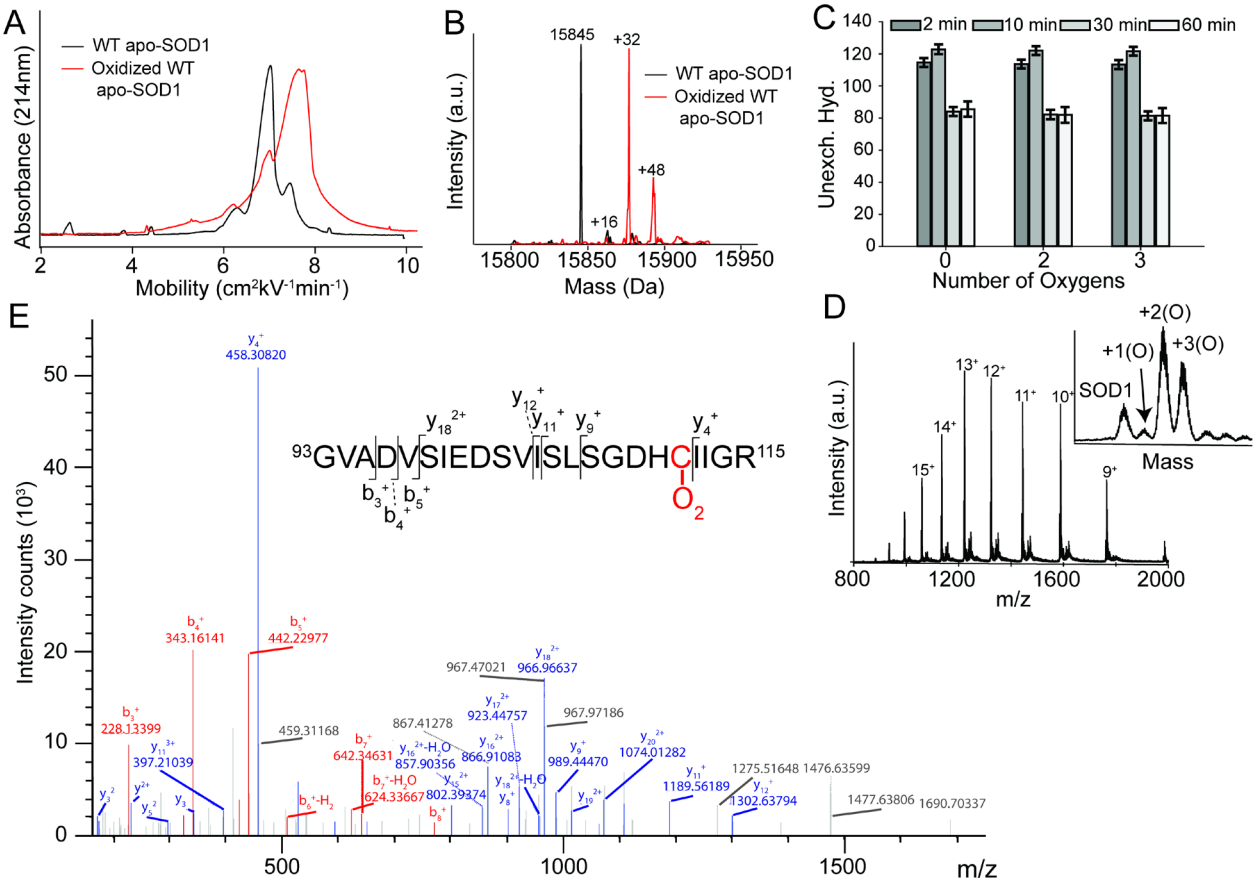

Figure 2. (A) Overlayed electropherograms of unoxidized human WT apo-SOD1 (black) and oxidized WT apo-SOD1 (red) in 10 mM potassium phosphate buffer, pH = 7.4. Addition of one unit of negative charge (per monomer) from oxidation of cysteine (to either Cys-SO_2^- or Cys-SO_3^-) increases electrophoretic mobility, whereas neutral oxidation products (i.e., 2-oxo-His, Cys-SOH) would not increase mobility. (B) Mass spectra of WT (black) and oxidized WT (red) apo-SOD1 were modified with either the addition of two oxygen (+32 Da) or three oxygen (+64 Da). (C) Unexchanged hydrogens after 2, 10, 30, and 60 min in amide H/D exchange of WT apo-SOD1 modified with hydrogen peroxide. Error bars represent standard deviation of three technical replicates. (D) Convoluted charge states of native and modified WT apo-SOD1 in water; deconvoluted mass spectrum inset. (E) MS/MS spectrum of tryptic fragment of oxidized WT apo-SOD1 showing Cys111 (red) oxidized to Cys-SO_2; X_{corr} = 4.02.

Table 1. Deconvoluted Mass Spectra for Oxidized and Unoxidized WT Apo-SOD1 in 90% D_2O

	MW[a] H_2O	MW $D_2O_{(60\ min)}$	MW $D_2O_{(denatured)}$	back exch. (%)[b]
SOD1-$C_{111}SH$	15844.06 ± 2.69	15906.43 ± 4.76	15948.66 ± 4.75	
SOD1-$C_{111}SO_2^-$	15876.04 ± 2.70	15942.00 ± 4.96	15985.37 ± 4.66	21.47 ± 5.46
SOD1-$C_{111}SO_3^-$	15892.14 ± 3.03	15958.42 ± 4.69	16002.99 ± 4.75	

[a]Each molecular weight (MW) is reported as an average, with standard deviation from three technical replicates. [b]Back exchange of deuterons calculated from most abundant peak in the mixture (SOD1-$C_{111}SO_2$)

apo-SOD1 (Table 1). Because the measurements of H/D exchange were made on the minute to hour time scale, it is possible (indeed likely) that cysteine oxidation perturbs structural elements that undergo H/D exchange on the time scale of seconds or milliseconds (e.g., disordered loops, surface regions, etc.).[25,57] Molecular dynamics simulations are used, below, to investigate this possibility.

Measuring Heterodimerization of Unoxidized ALS Mutant SOD1 with Oxidized WT SOD1. To initiate heterodimerization, oxidized WT apo-SOD1 and unoxidized E100K apo-SOD1 were combined in equal concentrations (60 μM total SOD1, determined by UV−vis). Prior to determination of protein concentration and heterodimerization, samples were washed with 10 mM potassium phosphate buffer (pH = 7.4) to remove residual H_2O_2. Note from the mass spectrum of oxidized WT SOD1 (Figure 2B) that C111 residues could not be oxidized completely from Cys-SO_2^- to Cys-SO_3^- with H_2O_2. However, both Cys-SO_3^- and Cys-SO_2^- are isoelectric and shift the electropherogram of WT apo-SOD1 in the same direction and by the same amount, resulting in a single broad peak composed of SOD1-SO_2^- and SOD1-SO_3^- (Figure 2A). The typical increase in electrophoretic mobility that we observed for WT apo-SOD1 and oxidized WT apo-SOD1 was $\Delta\mu$ = ~ 0.8−0.9 $cm^2\ kV^{-1}\ min^{-1}$ (Figure 2A). The theoretical increase in mobility was calculated to be $\Delta\mu$ = 0.77 $cm^2\ kV^{-1}\ min^{-1}$.

The mixtures of unoxidized mutant and oxidized-WT SOD1 (and controls of unoxidized mutant and unoxidized WT SOD1) were analyzed with CE immediately after mixing (Figure 3A−D). The appearance of a distinct middle peak in

https://doi.org/10.1021/acschemneuro.3c00174
ACS Chem. Neurosci. 2023, 14, 1547−1560

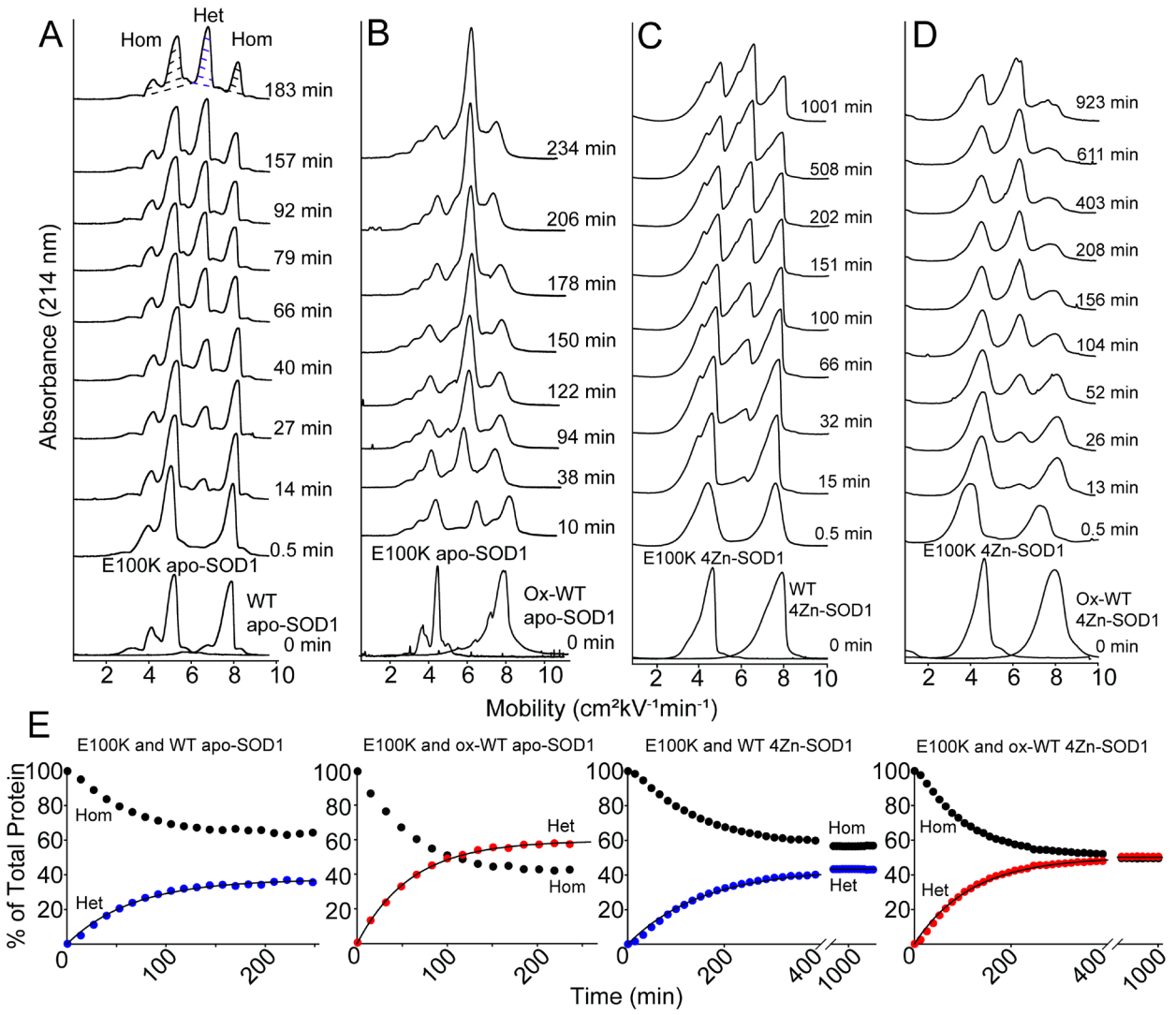

Figure 3. (A–D) Representative electropherograms of heterodimerization between (A) E100K and WT apo-SOD1(electropherogram at t = 183 min shows integration *via* the skim method), (B) E100K and oxidized WT apo-SOD1, (C) E100K and WT 4Zn-SOD1, and (D) E100K and oxidized WT 4Zn-SOD1. E. Increase in heterodimer and decrease in homodimers over time (homodimer = black, heterodimer = blue, unoxidized; red, oxidized). Each plot in E is directly below the electropherograms from which it was derived *via* integration of peaks for both homodimers and the heterodimer.

Table 2. Experimentally Determined Thermodynamic Parameters of SOD1 Heterodimerization

SOD1 mixture	SOD1 heterodimer	$t_{30\%}$ (min)	ΔG_{Het} (kJ/mol)
E100K + WT	apoE100K+apoWT	98.15 ± 13.39	−1.12 ± 0.16
	apoE100K+OxapoWT	38.29 ± 5.02	−6.23 ± 0.32
	ZnE100K+ZnWT	166.67 ± 5.29	−2.12 ± 0.03
	ZnE100K+ZnOxWT	107.52 ± 4.51	−4.01 ± 0.14
E100K + TD[a]	apoE100K+apoTD	72.71 ± 1.17	−2.76 ± 0.24
	apoE100K+OxapoTD	32.44 ± 1.42	−3.71 ± 0.48
	ZnE100K+ZnTD	177.39 ± 2.47	−2.51 ± 0.14
	ZnE100K+ZnOxTD	89.01 ± 1.93	−3.27 ± 0.39
WT + TD	apoWT+apoTD	78.89 ± 1.23	−2.20 ± 0.16
	apoWT+OxapoTD	31.23 ± 0.67	−3.79 ± 0.89
	OxapoWT+OxapoTD	88.71 ± 6.22	−1.63 ± 0.18
	ZnWT+ZnTD	279.43 ± 6.54	−1.48 ± 0.09
	ZnWT+ZnOxTD	92.54 ± 1.97	−2.99 ± 0.51

[a]TD = triply deamidated SOD1, simulated with the triple substitution: N26D/N131D/N139D.

the electropherogram, between the two homodimeric SOD1 species, was indicative of the heterodimer of E100K apo-SOD1 and WT apo-SOD1 (Figure 3A). The mobility of this emerging middle peak in each panel in Figure 3 (A–D) is

https://doi.org/10.1021/acschemneuro.3c00174
ACS Chem. Neurosci. 2023, 14, 1547−1560

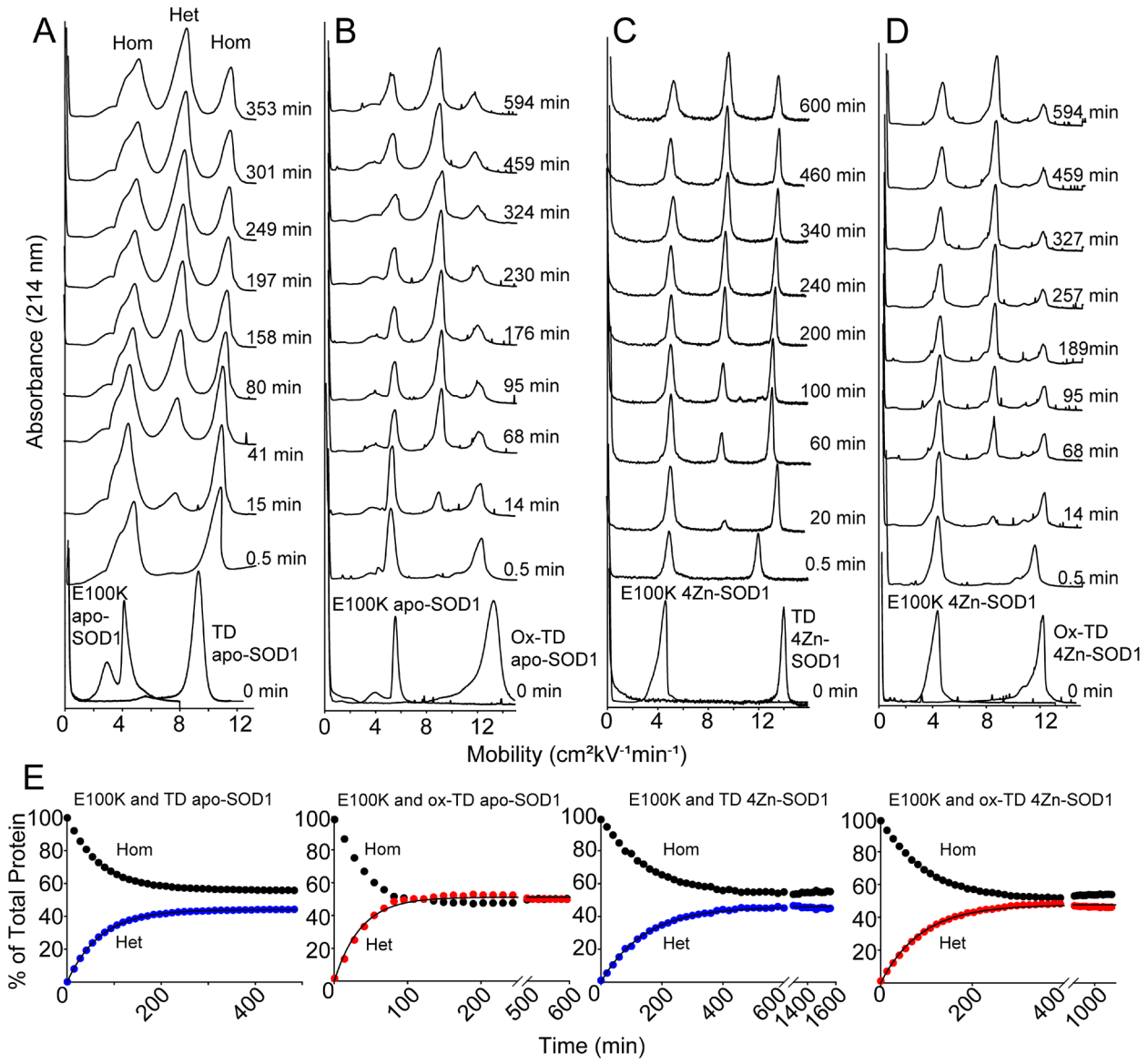

Figure 4. (A–D) Representative electropherograms of heterodimerization between (A) E100K and TD apo-SOD1, (B) E100K and oxidized TD apo-SOD1, (C) E100K and TD 4Zn-SOD1, and (D) E100K and oxidized TD 4Zn-SOD1. (E). Increase in heterodimer and decrease in homodimers over time (homodimer = black, heterodimer = blue, unoxidized; red, oxidized). Each plot in E is directly below the electropherograms from which it was derived *via* integration of peaks for both homodimers and the heterodimer.

equal to the predicted mobility of the heterodimer.[17] The integration of electrophoretic peaks of the E100K homodimer, WT homodimer, and WT/E100K heterodimer was performed using the skim method (Figure 3A, t = 183 min).[17] Longitudinal plots of increasing heterodimer and decreasing homodimers revealed that equilibrium was reached in ∼3–4 h for unoxidized E100K/WT apo-SOD1 and unoxidized E100K/oxidized WT apo-SOD1 (Figure 3E). The free energy of heterodimerization of unoxidized proteins was measured to be ΔG_{Het} = −1.12 ± 0.16 kJ mol^{-1} (similar to previous measurements carried out at slightly higher total concentrations of 100 μM[17]) (Table 2).

Note that the first time point in the longitudinal trace of heterodimerization is t = 0.5 min. After injection of the mixture of proteins into CE, there is an approximate dead time of 4–8 min before homodimers and heterodimers are detected *via* absorbance at 214 nm. By this time, however, heterodimerization is effectively quenched as both homodimers are separated from each other (unable to exchange subunits).

Heterodimerization of unoxidized E100K apo-SOD1 and oxidized WT apo-SOD1 was much more favorable compared to unoxidized heterodimers, with ΔG_{Het} = −6.23 ± 0.32 kJ mol^{-1} (Figure 3B,E and Table 2). Oxidation of C111 in WT apo-SOD1 also accelerated the rate of heterodimerization with E100K apo-SOD1 by ∼3-fold (e.g., the time for the mixture of homodimers to reach 30% heterodimer, $t_{30\%}$ = 98.15 ± 13.39 min for unoxidized E100K/unoxidized WT; $t_{30\%}$ = 38.29 ± 5.02 min for unoxidized E100K/oxidized WT) (Figure 3E and Table 2).

We also prepared oxidized E100K apo-SOD1 to examine its heterodimerization with unoxidized or oxidized WT SOD1. However, E100K apo-SOD1 underwent oxidation of additional residues besides C111 (Figure S1A) when oxidized with H_2O_2 under the same conditions as WT apo-SOD1. This oxidation involved the addition of eight oxygens. The electropherogram

https://doi.org/10.1021/acschemneuro.3c00174
ACS Chem. Neurosci. 2023, 14, 1547–1560

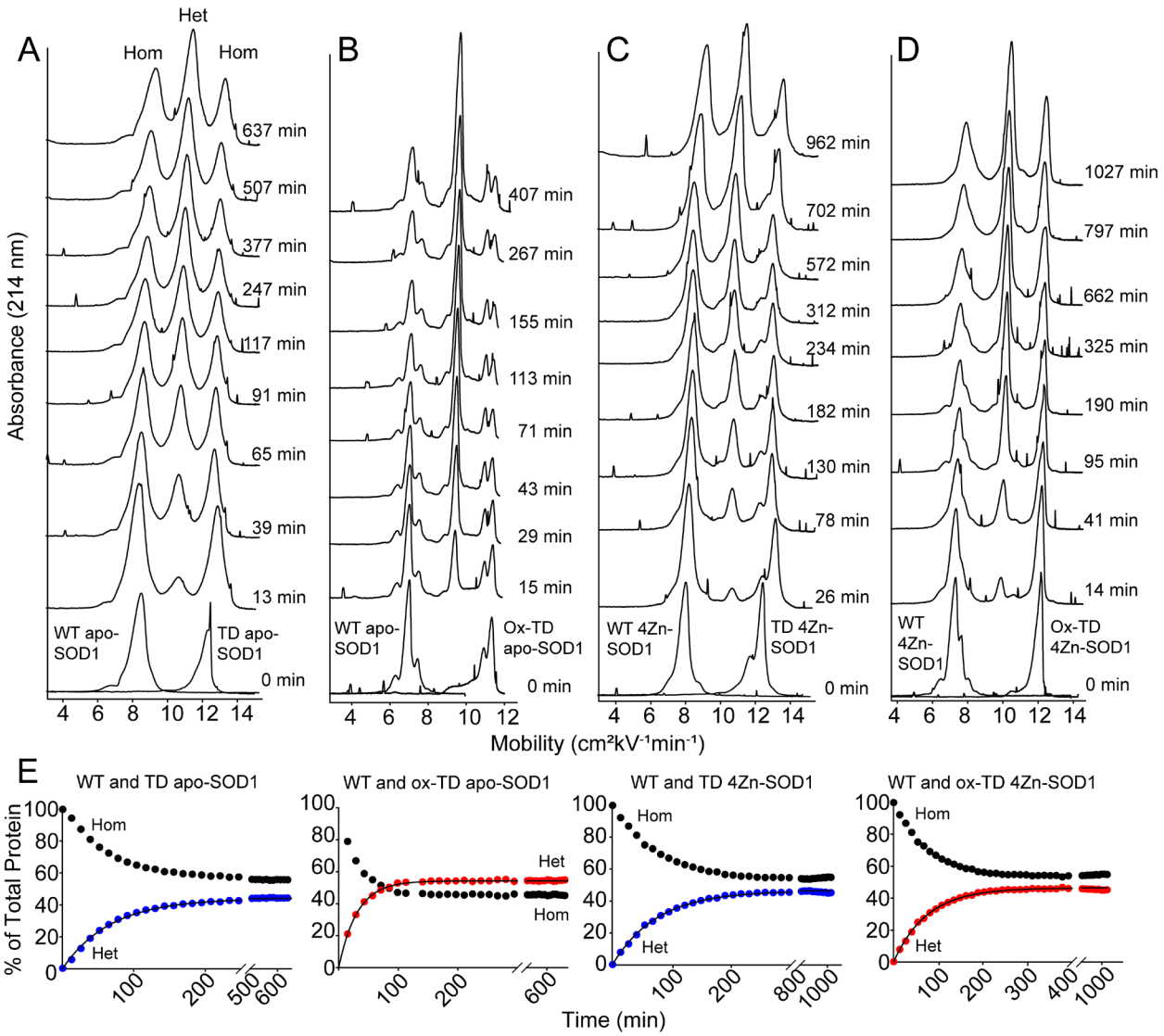

Figure 5. (A–D) Representative electropherograms of heterodimerization between (A) WT and TD apo-SOD1, (B) WT and oxidized TD apo-SOD1, (C) WT and TD 4Zn-SOD1, and (D) WT and oxidized TD 4Zn-SOD1. (E) Increase in heterodimer and decrease in homodimers over time (homodimer = black, heterodimer = blue, unoxidized; red, oxidized). Each plot in E is directly below the electropherograms from which it was derived *via* integration of peaks for both homodimers and the heterodimer.

of this hyper-oxidized protein was extremely broad (spanning 6 mobility units) and overlapped with WT SOD1 (i.e., 2.5–8.5 $cm^2\ kV^{-1}\ min^{-1}$; Figure S1B). Presumably, this broad mobility is due to oxidation-induced perturbations in structure that increase hydrodynamic drag or interactions with fused silica capillary. This prevented the examination of how C111-oxidized E100K apo-SOD1 heterodimerized with WT apo-SOD1.

Effect of Zn^{2+} Coordination on Heterodimerization of Oxidized and Unoxidized SOD1. To study how the coordination of Zn^{2+} to SOD1 attenuated the thermodynamic and kinetic effects of cysteine oxidation on heterodimerization, we prepared all SOD1 proteins (i.e., WT, E100K, and TD) with four stoichiometric equivalents of Zn^{2+} per dimer (4Zn-SOD1). Metal stoichiometries were verified with ICP-MS. Coordination of Zn^{2+} could be further verified with CE, by observing the expected decrease in electrophoretic mobility due to the lower magnitude of net negative charge[58] (Figure 3C,D). We did not examine heterodimerization of mixed metalation states, such as E100K apo-SOD1 with WT 4Zn-SOD1 but rather only studied heterodimerization of equivalent metalation states.

Compared to the heterodimerization of apo proteins, the rates of heterodimerization of unoxidized metalated proteins were much slower: $t_{30\%}$ = 166.67 ± 5.29 min for E100K and WT (Figure 3C,D and Table 2). Similar to the apo-SOD1, heterodimerization of unoxidized E100K 4Zn-SOD1 and oxidized WT 4Zn-SOD1 was more favorable compared to unoxidized heterodimers, with ΔG_{Het} = −4.01 ± 0.14 kJ mol^{-1} and ΔG_{Het} = −2.12 ± 0.03 kJ mol^{-1}, respectively (Figure 3C,D and Table 2). The data suggests that oxidation of C111 increases the rate of heterodimerization regardless of the metalation state of SOD1 (Figure 3B,D,E and Table 2). It is important to note, however, the promotional effects of cysteine oxidation seem to be reduced for metalated SOD1 ($\Delta\Delta G_{Het}$ = −1.89 ± 0.14 kJ mol^{-1} for E100K 4Zn-SOD1 and oxidized WT 4Zn-SOD1 relative to unoxidized counterparts whereas $\Delta\Delta G_{Het}$ = −5.11 ± 0.36 kJ mol^{-1} for E100K apo-SOD1 and oxidized WT apo-SOD1 relative to unoxidized counterparts) (Figure 3 and Table 2).

https://doi.org/10.1021/acschemneuro.3c00174
ACS Chem. Neurosci. 2023, 14, 1547–1560

Combined Effects of C111 Oxidation and N/D Substitutions on Heterodimerization. We are also interested in studying the deamidation of Asn to Asp in WT SOD1. This post-translational modification occurs to WT SOD1 *in vivo*[31,59] and is chemically equivalent to two ALS-linked SOD1 mutations, N139D and N86D. The deamidation of N139 or N86 is therefore pathogenic, *per se*.[5,60] Moreover, deamidation alters net charge in a manner that improves resolution of heterodimers during CE. Here, we mimic deamidation with Asn/Asp substitutions.

The three most rapidly deamidating Asn residues are predicted to be (in decreasing order of deamidation rate): N26, N131, and N139.[31] The predicted half-lives of deamidation of these Asn residues in native SOD1 are predicted to be 71, 351, and 1317 days.[31] Therefore, the slow component b axonal transport of holo-SOD1 down a one meter long motor neuron axon (requiring ~450 days) would result in SOD1 proteins that are 99% deamidated at N26, 55% at N131, and 21% for N139 (but only 1.7% at N86).[31] This triply deamidated form of WT might be physiologically relevant in persons that do not harbor ALS-linked SOD1 mutations, as well as those that do. Previous reports have detected the complete deamidation of N26 to aspartic acid in human SOD1 isolated from erythrocytes and in SOD1 peptides of the cerebrospinal fluid.[31,61] Recently, Double and co-workers detected deamidation in mutant SOD1 at N26, N131, and N53 (in post-mortem spinal cord of ALS patients).[59]

To examine how asparagine deamidation and cysteine oxidation—two modifications that form on the same WT SOD1 chain over time—affect heterodimerization, we used site directed mutagenesis to prepare an analogue of triply deamidated WT SOD1. This analogue contained the following three amino acid substitutions: N26D/N131D/N139D SOD1 (denoted "TD SOD1" for triply deamidated). The triple mutant apo-SOD1 protein was oxidized with H_2O_2 under the same conditions as WT apo-SOD1. Mass spectrometry confirmed the presence of predominantly two and three oxygens adducts (Figure S1C).

The unoxidized E100K apo-SOD1 protein was mixed with C111-oxidized TD apo-SOD1 (and separately, with unoxidized TD apo-SOD1) (Figure 4). Heterodimerization was measured with CE. The electropherogram yielded peaks that are highly resolved, as the two homodimers differ in formal net charge by 10 units, and the heterodimer differs in net charge from each homodimer by 5 units (Figure 4). Triple deamidation of unoxidized apo-SOD1 promoted heterodimerization with unoxidized E100K apo-SOD1 (Figure 4A), compared to WT apo-SOD1 (Figure 3A): $\Delta G_{Het} = -2.76 \pm 0.24$ kJ mol^{-1}; $\Delta\Delta G_{Het} = -1.64 \pm 0.29$ kJ mol^{-1} (Table 2). Triple deamidation accelerated heterodimerization, with $t_{30\%} = 72.71 \pm 1.17$ min (Table 2).

The oxidation of C111 in TD apo-SOD1 further promoted heterodimerization with E100K apo-SOD1 over the unoxidized TD apo-SOD1: $\Delta G_{Het} = -3.71 \pm 0.48$ kJ mol^{-1} ($\Delta\Delta G_{Het} = -0.95 \pm 0.54$ kJ mol^{-1}) (Figure 4B and Table 2). The oxidation of C111 in TD apo-SOD1 had a smaller effect on ΔG_{Het} with E100K SOD1 than the oxidation of C111 in WT apo-SOD1. The heterodimerization rate of unoxidized E100K apo-SOD1 and C111-oxidized TD apo-SOD1 yielded $t_{30\%} = 32.44 \pm 1.42$ min (Figure 4B and Table 2). Therefore, we conclude that triple deamidation of WT SOD1 partially offset the heterodimerizing effects of C111 oxidation in WT SOD1, regarding heterodimerization with ALS mutant SOD1.

Compared to the heterodimerization of apo proteins, the rates of heterodimerization of unoxidized metalated proteins were much slower: $t_{30\%} = 177.39 \pm 2.47$ min for E100K and TD (Figure 4C,D and Table 2). Heterodimerization of unoxidized E100K 4Zn-SOD1 and oxidized TD 4Zn-SOD1 was more favorable compared to unoxidized heterodimers, with $\Delta G_{Het} = -3.27 \pm 0.39$ kJ mol^{-1} and $\Delta G_{Het} = -2.51 \pm 0.14$ kJ mol^{-1}, respectively (Figure 4C,D and Table 2). Oxidation of C111 increased the rate of heterodimerization regardless of the metalation state of SOD1 as described above (Figure 4 and Table 2). The promotional effects of cysteine oxidation were also reduced for metalated SOD1 between this pair of SOD1 (Figure 4 and Table 2).

The high net negative charge of the triply deamidated apo-SOD1 protein allowed us to also measure its heterodimerization with the WT apo-SOD1 protein and determine how the oxidation of either affected heterodimerization (Figure 5). This pair is relevant to ALS as WT SOD1 has been linked to sporadic ALS.[62] The oxidation of C111 in TD apo-SOD1 promoted heterodimerization with WT apo-SOD1 (Figure 5B), compared to heterodimerization of both unoxidized proteins (Figure 5A): $\Delta G_{Het} = -3.79 \pm 0.89$ kJ mol^{-1} ($\Delta\Delta G_{Het} = -1.59 \pm 0.90$ kJ mol^{-1}) (Table 2). In contrast, the oxidation of both proteins disfavored heterodimerization, compared to the heterodimerization of both unoxidized proteins: $\Delta G_{Het} = -1.63 \pm 0.18$ kJ mol^{-1} ($\Delta\Delta G_{Het} = 0.57 \pm 0.24$ kJ mol^{-1}) (Table 2). This result is key to this study as it demonstrates that two SOD1 homodimers with C111 oxidized will not exchange subunits as readily as when only one dimer is oxidized. This suggests that C111 is not necessarily accelerating heterodimerization but destabilizing the oxidized homodimer (regardless of whether the oxidized homodimer is WT or mutant).

Compared to the heterodimerization of apo proteins, the rates of heterodimerization of unoxidized metalated proteins were much slower: $t_{30\%} = 279.43 \pm 6.54$ min for WT and TD (Figure 5 and Table 2). Heterodimerization of unoxidized WT 4Zn-SOD1 and oxidized TD 4Zn-SOD1 was more favorable compared to the unoxidized heterodimers, with $\Delta G_{Het} = -3.79 \pm 0.89$ kJ mol^{-1} and $\Delta G_{Het} = -2.20 \pm 0.16$ kJ mol^{-1}, respectively (Figure 5C,D and Table 2). Only a small decrease in ΔG_{Het} was observed with WT 4Zn-SOD1 and oxidized TD 4Zn-SOD1: $\Delta\Delta G_{Het} = -1.59 \pm 0.90$ kJ mol^{-1} (Table 2 and Figure 5). Oxidation of C111 increased the rate of heterodimerization regardless of the metalation state for all pairs of SOD1 in this study (Figures 3−5 and Table 2). Another observed trend was that the heterodimerization of metalated proteins, with one subunit oxidized, was generally less favorable than heterodimerization of the same proteins in the apo state (Figures 3−5 and Table 2).

We note that the oxidized TD apo-SOD1 protein migrated during CE, sometimes, as a doublet peak (Figures 4B and 5B). This doublet, which was fully included in integrations, is not likely caused by a mixture of metalation states as the metal content of the apo protein was found to be <0.1 Zn per dimer. This doublet has been observed at lower pH in SOD1 and might arise from different protonation states.[52,58]

If one assumes that, during the lifetime of metalated SOD1, the protein undergoes cysteine oxidation, and eventual loss of metal ions, then our results suggest that heterodimerization of SOD1 becomes more favorable during its lifetime (Figure 6).

https://doi.org/10.1021/acschemneuro.3c00174
ACS Chem. Neurosci. 2023, 14, 1547−1560

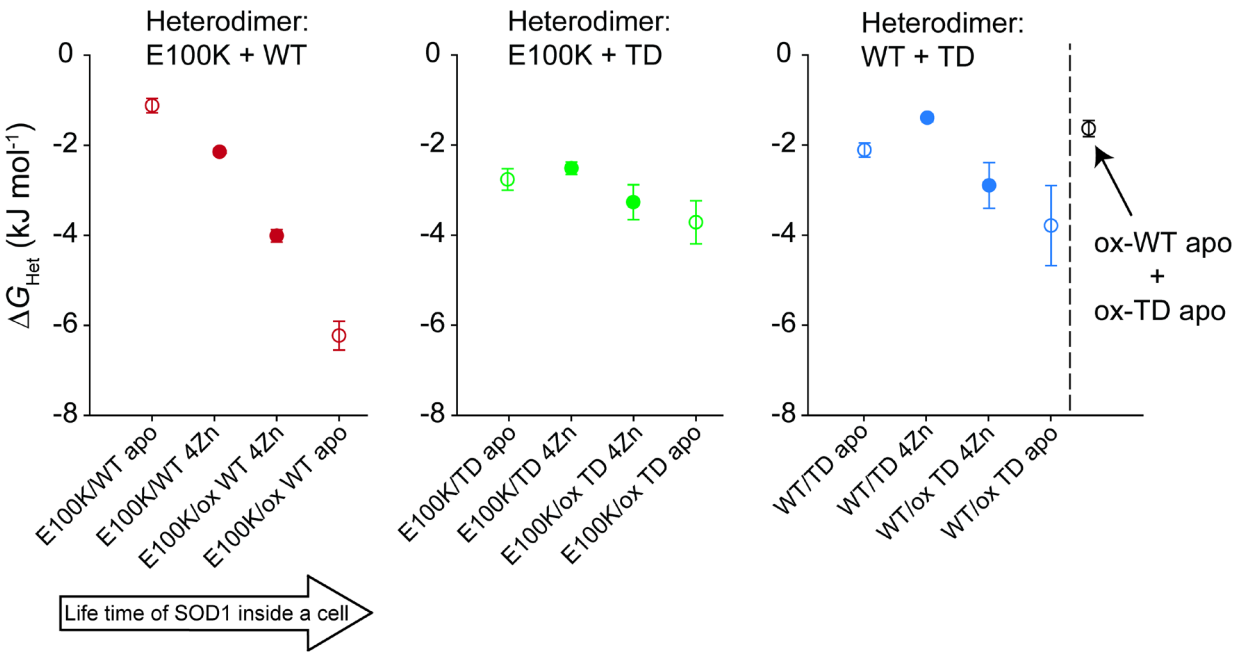

Figure 6. Measured ΔG_{Het} of different heterodimers of wild-type (WT) SOD1, E100 K SOD1, and triply deamidated (TD) SOD1 (i.e., N26D/N131D/N139D). The *x*-axis of each panel proceeds from a metal free SOD1 protein, to fully metalated SOD1, to oxidized and fully metalated SOD1, to a metal free heterodimer with one oxidized subunit. The oxidized subunit in the heterodimer is denoted with "ox". This post-translational progression, and corresponding decrease in ΔG_{Het} might mimic the lifetime of SOD1 in a motor neuron. The far right data point of the far right panel (black) represents ΔG_{Het} of WT and TD apo-SOD1 when both subunits are oxidized at C111. Error bars represent standard deviation.

Table 3. Molecular Dynamic Trajectories of Nonbonded Interaction Energies between Protein Subunits upon Oxidation of C111 on WT apo-SOD1 Subunit in Homodimer and Heterodimer with E100 K apo-SOD1[a]

	homodimer			heterodimer		
structure	Coulombic (kJ/mol)	vdW (kJ/mol)	total (kJ/mol)	Coulombic (kJ/mol)	vdW (kJ/mol)	total (kJ/mol)
unmodified (SH)	−186 ± 95	−321 ± 18	−507 ± 99	−152 ± 88	−318 ± 18	−469 ± 92
sulfenic (SO^-)	−78 ± 83	−321 ± 18	−399 ± 87	−114 ± 76	−318 ± 17	−433 ± 80
sulfinic (SO_2^-)	−84 ± 78	−317 ± 18	−401 ± 82	−150 ± 89	−318 ± 18	−468 ± 93
sulfonic (SO_3^-)	−146 ± 90	−324 ± 18	−470 ± 95	−137 ± 81	−323 ± 18	−460 ± 84

[a]Energies are expressed as averages ± standard deviations.

Table 4. Molecular Dynamic Trajectories of Non-Bonded Interaction Energies between Both C111 Residues in WT apo-SOD1 Subunit in Homodimer and Heterodimer with E100K apo-SOD1[a]

	homodimer			heterodimer		
structure	Coulombic (kJ/mol)	vdW (kJ/mol)	total (kJ/mol)	Coulombic (kJ/mol)	vdW (kJ/mol)	total (kJ/mol)
unmodified (SH)	0.1 ± 0.4	−0.1 ± 0.0	0.0 ± 0.4	0.1 ± 0.0	−0.1 ± 0.0	0.1 ± 0.4
sulfenic (SO^-)	46 ± 18	−0.2 ± 0.1	45 ± 18	−3.5 ± 3.2	−0.1 ± 0.0	−3.6 ± 3.2
sulfinic (SO_2^-)	33 ± 13	−0.2 ± 0.1	33 ± 13	−3.1 ± 2.8	−0.1 ± 0.0	−3.2 ± 2.9
sulfonic (SO_3^-)	29 ± 11	−0.3 ± 0.1	29 ± 11	−2.8 ± 2.2	−0.1 ± 0.0	−2.9 ± 2.2

[a]Only C111 on the WT apo-SOD1 subunit was oxidized. Energies are expressed as averages ± standard deviations.

However, the substitution of three specific Asn residues to Asp appears to dampen (but not abolish) this drive toward heterodimerization (Figure 6). Since most ALS individuals are heterozygous, WT and mutant SOD1 are coexpressed. Considering the extent to which E100 K SOD1 was oxidized, it is likely that this mutant would be oxidized at a higher rate compared to WT SOD1. This would destabilize the E100 K homodimer and drive the heterodimerization between mutant and WT SOD1.

Mechanism of Cys-SO_x Induced Subunit Swapping. The proper conclusion to this study would be to elucidate a structural or atomic-level mechanism for Cys-SO_2^-/SO_3^- mediated subunit swapping/heterodimerization. Elucidating such a mechanism is difficult with experiment. Isolating heterodimers from preceding homodimers to allow structural or biophysical analysis is nearly impossible, without covalent trapping/cross-linking. Therefore, we used molecular dynamic simulations to predict possible structural and/or electrostatic mechanisms for oxidation-induced heterodimerization.

The majority of the oxidized WT SOD1 protein that we studied (experimentally, with CE) contained sulfinic acid (with minor amounts of sulfenic and sulfonic groups, according to mass spectrometry; Figure 2). Nevertheless, we parametrized all four states of cysteine oxidation for MD simulations (i.e.,

https://doi.org/10.1021/acschemneuro.3c00174
ACS Chem. Neurosci. 2023, 14, 1547−1560

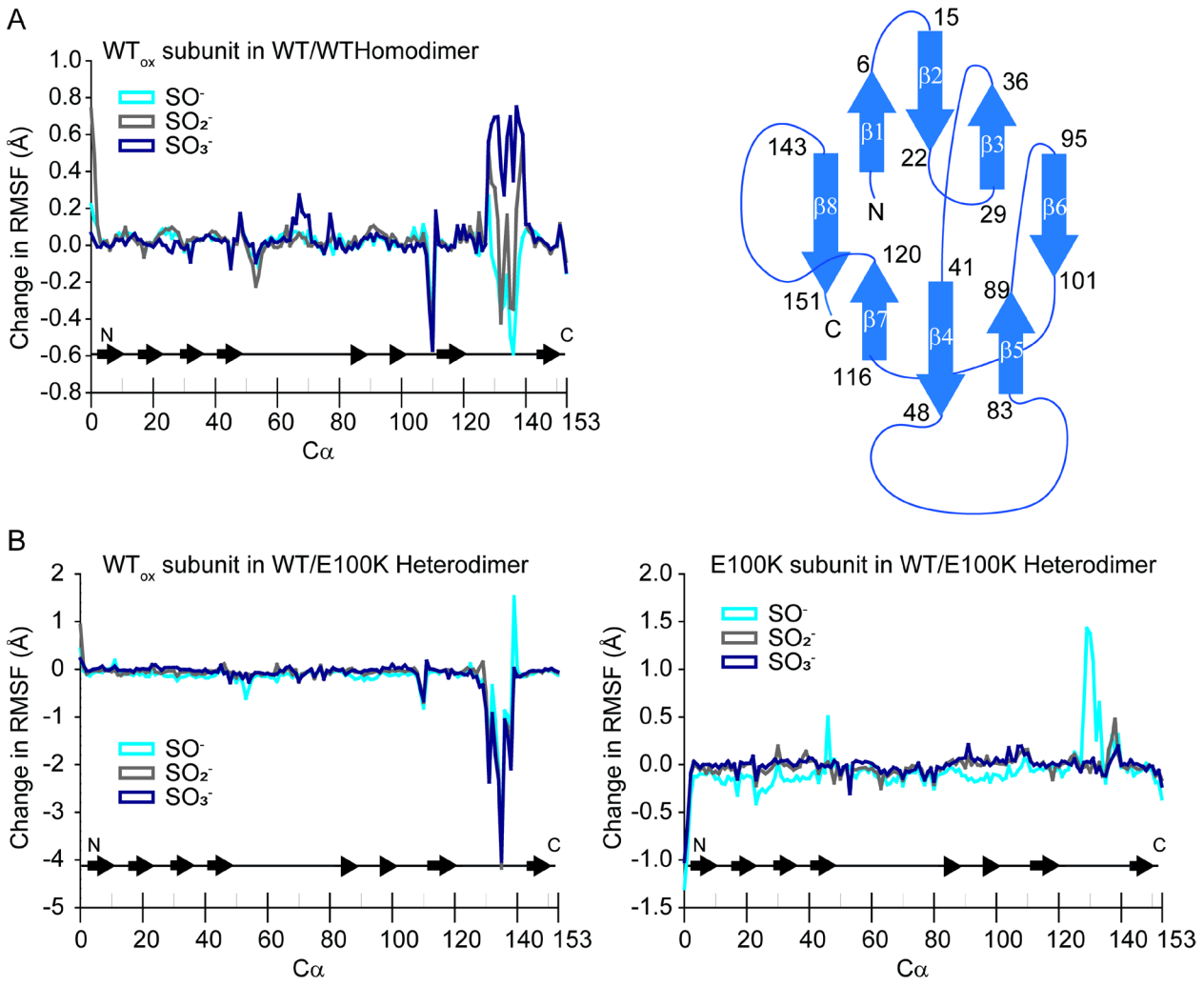

Figure 7. Root mean standard fluctuation (RMSF) plots for WT apo-SOD1 homodimer and WT/E100K apo-SOD1 heterodimer in unoxidized and oxidized states. (A) Changes in RMSF upon oxidation of C111 on the WT subunits in the WT apo-SOD1 homodimer. Fluctuation is expressed relative to the unoxidized homodimer. A secondary structure map is shown to illustrate where each residue is located in terms of the native structure of SOD1. (B) Changes in RMSF upon oxidation of C111 on the WT subunit in the WT/E100K apo-SOD1 heterodimer. Fluctuation is expressed for each subunit relative to its position in the unoxidized heterodimer.

unoxidized sulfhydryl, sulfenic, sulfinic, and sulfonic acid). It is possible that sulfonic or sulfenic groups have greater effects on heterodimerization (than sulfinic groups), which might outweigh their minor abundance.

Calculation of Coulombic interaction energies between subunits of the oxidized homodimers and heterodimers (of oxidized WT and unoxidized mutant SOD1) predicts that oxidation to sulfinic acid destabilizes the WT homodimer (electrostatically) by 2-fold, without significantly altering the van der Waals forces between homodimer subunits (Tables 3 and 4). However, these calculations suggest that oxidation of C111 in WT does not alter its Coulombic interaction energy with the unoxidized E100 K subunit of the heterodimer (and does not alter the van der Waals interaction energy; Tables 3 and 4).

We can speculate from these data—in terms of electrostatics—that the oxidation of C111 in WT SOD1 promotes heterodimerization with unoxidized E100K SOD1 by destabilizing the oxidized WT SOD1 homodimer and not necessarily by stabilizing the WT/E100K heterodimer. This hypothesis seems reasonable when considering the close proximity of the two "dueling" C111 residues at the dimer interface. It is possible that the close distance facilitates electrostatic repulsion upon oxidation, which is relieved by heterodimerization with an unoxidized subunit. This electrostatic repulsion and destabilization of the oxidized WT homodimer supports the free energies determined by CE. These findings are extremely important in understanding the heterodimerization between mutant and WT SOD1. For mutants that act similarly to E100K in terms of their propensity for oxidative damage, this likely has large physiological implications.

We reason that the sulfenic/sulfinic groups are more potent at electrostatically destabilizing the homodimer than sulfonic groups (Tables 3 and 4) because the addition of oxygen atoms allows for delocalization of negative charge, thus reducing the electrostatic repulsion to some degree (Table 3). We also point out that the unrealistically large absolute values of the electrostatic energy in Table 3 are typical in these types of calculations. These large electrostatic energy values can be attributed to the greater sensitivity of a fixed point-charge electrostatics model to instantaneous environmental conformations.[63] The changes in the electrostatic energy upon oxidation for the heterodimer compared to the homodimer are more relevant.

https://doi.org/10.1021/acschemneuro.3c00174
ACS Chem. Neurosci. 2023, 14, 1547−1560

Molecular dynamics also predicted that the root mean squared deviation (RMSD) of atoms in the backbone of oxidized and unoxidized dimers (*in silico*) is generally less than 2 Å. This simulation suggests that C111 oxidation does not significantly alter the overall structure of SOD1 in any homo- or heterodimeric state (Figure S2). The radius of gyration (RoG) supports this conclusion as no fluctuations were observed (Figure S3). According to these simulations, neither subunit (WT or E100K) were predicted to have large structural changes upon oxidation of C111 on the WT subunit, and both WT homodimer and WT/E100K retained their overall structure.

A closer look, at the amino acid level, does suggest some minor structural perturbations upon heterodimerization. For example, the difference of the average root mean squared fluctuation (ΔRMSF) of amino acids in the E100K/unoxidized WT apo-SOD1 heterodimer and E100K/oxidized WT apo-SOD1 heterodimer suggested that C111 oxidation caused significant local perturbations in residues 126−135 of both the WT and E100K subunits (Figure 7). These residues make up part of the electrostatic loop of SOD1 (Figure 7A). Here, oxidation of C111 caused a significant tightening of residues in the electrostatic loop of WT SOD1 (illustrated by the largest negative ΔRMSF of −4 Å) and a small loosening in the E100K mutant (Figure 7B). Similar analysis of the oxidized and unoxidized WT apo-SOD1 homodimer showed that oxidation caused no significant perturbations in the structure of the WT apo-SOD1 homodimer (Figure 7A). These latter data are supported by the similar rates of amide H/D exchange of the oxidized and unoxidized WT SOD1 homodimers (Figure 2C).

In summary, these MD simulations suggest—but by no means prove—that the oxidation of C111 promotes subunit exchange through electrostatic destabilization of the homodimer, rather than novel stabilization of the new heterodimer. These simulations provide a starting point to understand the profound effect that C111 exerts on the heterodimerization (and perhaps toxicity) of WT and mutant SOD1. This idea is furthered when considering mutant SOD1 may have a higher tendency to become oxidized. If both mutant and WT SOD1 were oxidized at a similar rate, the effects of increased heterodimerization would not be seen.

Conclusion. This study suggests that cysteine oxidation promotes subunit swapping between oxidized and nonoxidized SOD1 dimers. It is possible that this promotional effect of cysteine oxidation on subunit swapping is independent of whether the mutant or WT protein is being oxidized (i.e., oxidatin simply promotes exchange of an oxidized subunits with unoxidized subunits, whether they be mutant or WT).

Cysteine-111 is already known to be one of many critical residues in the aggregation and neurotoxicity of SOD1, as it is the site of one known ALS missense mutation (C111Y).[64−66] Cysteine-111 is also readily modified with glutathione,[28] which can mediate SOD1 aggregation[67] (and substitution of C111 to Ser111 can prevent the formation of non-native intermolecular disulfide bonds between free C111 during covalent aggregation[68−70]).

The results of this study suggest that C111 also plays a direct role in controlling the exchange of SOD1 subunits, in a redox-dependent manner. As much as the heterodimerization of mutant and WT SOD1 drives their toxicity, it is reasonable to hypothesize that any process that promotes oxidation of C111 (such as oxidative stress[71−73]) could promote pathogenesis of SOD1 in ALS. Indeed, the SOD1 protein is a constant target of oxidation in that both its reactants and products are oxidants of cysteine, which provides a link between oxidative stress and SOD1 misfolding linked to ALS.[74−77] This link has been targeted therapeutically.[78−80] This study identifies an additional mechanism by which oxidative stress might promote the aggregation and neurotoxicity of mutant and WT SOD1, by amplifying the heterodimeric interaction between these two proteins. Of course, this mechanism relies on one of the homodimers (in this case E100K) to be oxidized preferentially as oxidation of both homodimers would not yield accelerated heterodimerization. If one assumes that, during the lifetime of metalated, mutant SOD1, the protein undergoes cysteine oxidation, and eventual loss of metal ions, then our results suggest that heterodimerization of SOD1 becomes more favorable during its lifetime. However, our results suggest that the deamidation of three asparagine—a natural post translational modification that occurs to SOD1 over time—also appears to dampen the drive toward heterodimerization.

EXPERIMENTAL PROCEDURES

Purification and Demetalation of SOD1. Superoxide dismutase 1 (WT or mutant) was recombinantly expressed in *S. cervisiae*. The SOD1 proteins were purified using successive ammonium sulfate precipitation, hydrophobic interaction chromatography, ion exchange chromatography, and size exclusion chromatography, as previously described.[81] The resulting protein solution was verified to contain SOD1 *via* SDS-PAGE following each chromatographic step of purification. Once purified, SOD1 was demetalated *via* sequential dialysis in (1) 0.1 M sodium acetate, 10 mM EDTA pH 3.8, (2) 0.1 M sodium acetate, 10 mM NaCl pH 3.8, and (3) 0.1 M sodium acetate pH 5.5. Full demetalation of SOD1 was verified with inductively coupled plasma-mass spectrometry (7900 ICP-MS, Agilent Technologies).

Oxidation of Cysteine in SOD1. Solutions of SOD1 (100 μM dimer, 10 mM potassium phosphate buffer, pH = 7.4) were incubated with 25 mM hydrogen peroxide over 48 h at 23 °C. The mixture was subsequently washed with 10 mM potassium phosphate buffer *via* centrifugal filtration to remove excess hydrogen peroxide. Oxidation was verified *via* mass spectrometry.

Capillary Electrophoresis (CE). All CE experiments were performed using an AB Sciex P/ACE MDQ *plus* equipped with a bare fused-silica capillary. Each CE experiment solution composed of 1 μL of 0.1 M DMF as neutral marker as electroosmotic flow (EOF) and mixture of protein and running buffer to ensure protein solutions were kept at approximately 60 μM. Experiments were performed at 29 kV at 22 °C, and each electrophoresis was carried out over a period of 13−20 min. After each individual experiment, the capillary was washed with 0.1 M potassium hydroxide, Milli-Q water, sequentially for 2 min each and finally reconditioned with the running buffer for 1 min.

Origin software was used to integrate the area of each peak (two homodimer and one heterodimer) in the electropherograms (Figures 3−5A−D). These integrations were summed and used to determine the stoichiometric fraction (expressed as a percentage) of each homo or heterodimeric state (Figures 3−5E). Upon equilibrium (when curve of each peak plateaus), the K_{Het} can be calculated using K_{Het} = [Heterodimer]2/([$WT_{homodimer}$][$ALS_{homodimer}$]). ΔG_{Het} was then calculated using $\Delta G_{Het} = -RT \ln K_{Het}$. The reported ΔG_{Het} represents the average of ΔG_{Het} calculated from the last three time points on the kinetic plots (Figures 3−5E) with standard deviation reported. $\Delta\Delta G_{Het}$ was calculated using (ΔG_{Het} of oxidized) − (ΔG_{Het} of unmodified SOD1), and propagation of error was used to calculate the standard deviation.

Mass Spectrometry. Oxidized apo SOD1 were diluted in 0.2% formic acid, and 200 μL was loaded onto a desalting trap column. A sample was injected into an Orbitrap Discovery, desalted with 500 mL of 0.2% formic acid, and then eluted with a solution of 80%

https://doi.org/10.1021/acschemneuro.3c00174
ACS Chem. Neurosci. 2023, 14, 1547−1560

acetonitrile, 19.8% H_2O, and 0.2% formic acid. Mass spectra were deconvoluted with MaxEnt1 module in MassLynx software.

Hydrogen/Deuterium Exchange. A 100 μL aliquot of the oxidized samples were diluted into 900 μL of 99.9% D_2O (Cambridge Isotope Laboratories, Inc., Tewksbury, MA). After 60 min of incubation at 22 °C, 50 μL of the solution was removed and flash frozen in liquid nitrogen (to quench H/D exchange) and stored at −80 °C until mass spectrometric analysis. The remaining solution was placed on a heat block (preheated to 90 °C) for 5 min to generate a perdeuterated sample (to quantify hydrogen back-exchange). A 50 μL aliquot of each sample was flash frozen as well for mass spectrometric analysis. Frozen aliquots were removed from the freezer and instantly thawed by the addition of 950 μL of ice-chilled H_2O (2.0% formic acid). The diluted samples were immediately loaded onto a desalting column (Michrom BioResources, Inc., Auburn, CA) and washed with 2 mL of cold H_2O (2.0% formic acid) before eluting with an 80:18:2 mixture of acetonitrile, water, and formic acid. Each measurement was made in approximately 5 min from time of thawing (2.5 min sample preparation and loading time, 2.5 min data collection). An Orbitrap Discovery instrument was used for all H/D exchange experiments.

Mass Spectrometry of Tryptic Fragments. Tryptic digests of oxidized protein solutions were generated *via* incubation with (i) dithiothreitol (DTT; 2 mM) and (ii) Trypsin Gold (Promega, WI, USA) at a ratio of 1:20 (trypsin/acylated protein). DTT was added to each protein sample and incubated at RT for 1 h. Trypsin was then added, and the digest mixture was incubated at 37 °C for ∼24 h. Trypsin digestion was performed in 50 mM Tris-HCl buffer (pH 8.8). A Q-Exactive Focus Orbitrap instrument was used to acquire mass spectra for peptides. Proteomic analysis of mass spectra and MS/MS spectra was performed using SeQuest in the Proteome Discoverer software.

Molecular Dynamics Simulations. A total of >5 μs of production-stage molecular dynamics in the *NPT* ensemble at 300 K and 1.0 bar were performed for (1) wild-type (WT) homodimers, in which the side chain of Cys-111 on each subunit was $-CH_2SH$, $-CH_2SO^-$, $-CH_2SO_2^-$, or $-CH_2SO_3^-$, and (2) WT-E100K heterodimers, in which the side chain of Cys-111 on the WT subunit was $-CH_2SH$, $-CH_2SO^-$, $-CH_2SO_2^-$, or $-CH_2SO_3^-$. All homo/heterodimers were modeled in the apo state. The oxidized Cys residues were parametrized in a manner consistent with the AMBER ff99SB force field used for the rest of the protein. Details regarding the parametrization strategy, as well as the setup and equilibration protocol for the molecular dynamics simulations are given in the Supportong Information (SI).

The structural stability and conformational mobility of the proteins as a function of time or Cys-111 oxidation were monitored by computing the backbone root-mean-squared deviation (RMSD; Figure S2), the per-residue root-mean-squared fluctuation (RMSF; Figure 7), and the radius of gyration (RoG; Figure S3). The energetic consequence for heterodimerization from Cys-111 oxidation was examined by computing the change in nonbonded interactions (Coulombic + van der Waals) either between protein subunits or only the Cys-111 residue on the two subunits (Tables 3 and 4). A relative metric for the change in nonbonded interactions upon heterodimerization was obtained by the application of eq 1 to the data of Tables 3 and 4.

$$\Delta\Delta E_{\text{non-bonded}} = ((\text{XM} - \text{XX}) - ((\text{UM} - \text{UU})) \quad (1)$$

where U = unoxidized wild-type, M = E100K mutant, and X = oxidized wild-type subunit. In agreement with the experiments reported in the present work, this was negative, to a different extent, for each oxidized Cys-111 side chain.

■ ASSOCIATED CONTENT

Data Availability Statement

All data are contained within the manuscript.

Supporting Information

The Supporting Information is available free of charge at https://pubs.acs.org/doi/10.1021/acschemneuro.3c00174.

Figures of mass spectra of E100K before and after incubation in H_2O_2 and plots of RMSD and RoG for WT apo-SOD1 homodimer and WT/E100K apo-SOD1 heterodimer and discussions of parametrization for cystine oxidation states, molecular dynamics simulations, and analyses[82−101] (PDF)

■ AUTHOR INFORMATION

Corresponding Author

Bryan F. Shaw − *Department of Chemistry and Biochemistry, Baylor University, Waco, Texas 76706, United States;* orcid.org/0000-0001-8265-5833; Email: bryan_shaw@baylor.edu

Authors

Ao Yun Zhang − *Department of Chemistry and Biochemistry, Baylor University, Waco, Texas 76706, United States*

Chad M. Dashnaw − *Department of Chemistry and Biochemistry, Baylor University, Waco, Texas 76706, United States;* orcid.org/0000-0002-7662-6611

Mayte Gonzalez − *Department of Chemistry and Biochemistry, Baylor University, Waco, Texas 76706, United States*

Jordan C. Koone − *Department of Chemistry and Biochemistry, Baylor University, Waco, Texas 76706, United States;* orcid.org/0000-0003-2021-5298

Nick A. Wells − *Department of Chemistry, Wesleyan University, Middletown, Connecticut 06459, United States;* orcid.org/0000-0002-5901-1594

Colin A. Smith − *Department of Chemistry, Wesleyan University, Middletown, Connecticut 06459, United States;* orcid.org/0000-0002-4651-167X

Matthew J. Guberman-Pfeffer − *Department of Chemistry and Biochemistry, Baylor University, Waco, Texas 76706, United States*

Complete contact information is available at: https://pubs.acs.org/10.1021/acschemneuro.3c00174

Author Contributions

[§]A.Y.Z. and C.M.D. contributed equally to this work.

Funding

This research was supported by grants from the National Science Foundation (CHE: 2203441) and Welch Foundation (AA-1854).

Notes

The authors declare no competing financial interest.

■ REFERENCES

(1) Sheng, Y.; Abreu, I. A.; Cabelli, D. E.; Maroney, M. J.; Miller, A. F.; Teixeira, M.; Valentine, J. S. Superoxide dismutases and superoxide reductases. *Chem. Rev.* **2014**, *114* (7), 3854−918.

(2) Wright, G. S. A.; Antonyuk, S. V.; Hasnain, S. S. The biophysics of superoxide dismutase-1 and amyotrophic lateral sclerosis. *Quart. Rev. Biophys.* **2019**, *52*, e12.

(3) Muller, K.; Oh, K. W.; Nordin, A.; Panthi, S.; Kim, S. H.; Nordin, F.; Freischmidt, A.; Ludolph, A. C.; Ki, C. S.; Forsberg, K.; Weishaupt, J.; Kim, Y. E.; Andersen, P. M. De novo mutations in SOD1 are a cause of ALS. *J. Neurol., Neurosurg. Psychiatry* **2022**, *93* (2), 201−206.

(4) Feldman, E. L.; Goutman, S. A.; Petri, S.; Mazzini, L.; Savelieff, M. G.; Shaw, P. J.; Sobue, G. Amyotrophic lateral sclerosis. *Lancet* **2022**, *400* (10360), 1363−1380.

(5) Bystrom, R.; Andersen, P. M.; Grobner, G.; Oliveberg, M. SOD1 mutations targeting surface hydrogen bonds promote amyotrophic lateral sclerosis without reducing apo-state stability. *J. Biol. Chem.* **2010**, *285* (25), 19544−52.
(6) Wang, Q.; Johnson, J. L.; Agar, N. Y.; Agar, J. N. Protein aggregation and protein instability govern familial amyotrophic lateral sclerosis patient survival. *PLoS Biol.* **2008**, *6* (7), e170.
(7) Juneja, T.; Pericak-Vance, M. A.; Laing, N. G.; Dave, S.; Siddique, T. Prognosis in familial amyotrophic lateral sclerosis: progression and survival in patients with glu100gly and ala4val mutations in Cu,Zn superoxide dismutase. *Neurology* **1997**, *48* (1), 55−7.
(8) Bali, T.; Self, W.; Liu, J.; Siddique, T.; Wang, L. H.; Bird, T. D.; Ratti, E.; Atassi, N.; Boylan, K. B.; Glass, J. D.; Maragakis, N. J.; Caress, J. B.; McCluskey, L. F.; Appel, S. H.; Wymer, J. P.; Gibson, S.; Zinman, L.; Mozaffar, T.; Callaghan, B.; McVey, A. L.; Jockel-Balsarotti, J.; Allred, P.; Fisher, E. R.; Lopate, G.; Pestronk, A.; Cudkowicz, M. E.; Miller, T. M. Defining SOD1 ALS natural history to guide therapeutic clinical trial design. *J. Neurol., Neurosurg. Psychiatry* **2017**, *88* (2), 99−105.
(9) Rosen, D. R.; Bowling, A. C.; Patterson, D.; Usdin, T. B.; Sapp, P.; Mezey, E.; Mckennayasek, D.; O'Regan, J.; Rahmani, Z.; Ferrante, R. J.; Brownstein, M. J.; Kowall, N. W.; Beal, M. F.; Horvitz, H. R.; Brown, R. H. A Frequent Ala-4 to Val Superoxide Dismutase-1 Mutation Is Associated with a Rapidly Progressive Familial Amyotrophic-Lateral-Sclerosis. *Hum. Mol. Genet.* **1994**, *3* (6), 981−987.
(10) Steenland, K.; MacNeil, J.; Seals, R.; Levey, A. Factors affecting survival of patients with neurodegenerative disease. *Neuroepidemiology* **2010**, *35* (1), 28−35.
(11) Mackay, D. F.; Russell, E. R.; Stewart, K.; MacLean, J. A.; Pell, J. P.; Stewart, W. Neurodegenerative Disease Mortality among Former Professional Soccer Players. *N. Engl. J. Med.* **2019**, *381* (19), 1801−1808.
(12) Chen, W. J.; Cheng, X. W.; Fu, Y.; Zhao, M.; McGinley, J.; Westenberger, A.; Xiong, Z. Q. Rethinking monogenic neurological diseases. *BMJ [Br. Med. J.]* **2020**, *371*, m3752.
(13) de Lau, L. M.; Schipper, C. M.; Hofman, A.; Koudstaal, P. J.; Breteler, M. M. Prognosis of Parkinson disease: risk of dementia and mortality: the Rotterdam Study. *Arch. Neurol.* **2005**, *62* (8), 1265−9.
(14) Liang, C.-S.; Li, D.-J.; Yang, F.-C.; Tseng, P.-T.; Carvalho, A. F; Stubbs, B.; Thompson, T.; Mueller, C.; Shin, J. I.; Radua, J.; Stewart, R.; Rajji, T. K; Tu, Y.-K.; Chen, T.-Y.; Yeh, T.-C.; Tsai, C.-K.; Yu, C.-L.; Pan, C.-C.; Chu, C.-S. Mortality rates in Alzheimer's disease and non-Alzheimer's dementias: a systematic review and meta-analysis. *Lancet Health Longev.* **2021**, *2* (8), E479−E488.
(15) Sandelin, E.; Nordlund, A.; Andersen, P. M.; Marklund, S. S.; Oliveberg, M. Amyotrophic lateral sclerosis-associated copper/zinc superoxide dismutase mutations preferentially reduce the repulsive charge of the proteins. *J. Biol. Chem.* **2007**, *282* (29), 21230−6.
(16) Shaw, B. F.; Valentine, J. S. How do ALS-associated mutations in superoxide dismutase 1 promote aggregation of the protein? *Trends. Biochem. Sci.* **2007**, *32* (2), 78−85.
(17) Shi, Y.; Acerson, M. J.; Abdolvahabi, A.; Mowery, R. A.; Shaw, B. F. Gibbs Energy of Superoxide Dismutase Heterodimerization Accounts for Variable Survival in Amyotrophic Lateral Sclerosis. *J. Am. Chem. Soc.* **2016**, *138* (16), 5351−62.
(18) Brasil, A. A.; de Carvalho, M. D. C.; Gerhardt, E.; Queiroz, D. D.; Pereira, M. D.; Outeiro, T. F.; Eleutherio, E. C. A. Characterization of the activity, aggregation, and toxicity of heterodimers of WT and ALS-associated mutant Sod1. *Proc. Natl. Acad. Sci. U.S.A.* **2019**, *116* (51), 25991−26000.
(19) Wang, L.; Deng, H. X.; Grisotti, G.; Zhai, H.; Siddique, T.; Roos, R. P. Wild-type SOD1 overexpression accelerates disease onset of a G85R SOD1 mouse. *Hum. Mol. Genet.* **2009**, *18* (9), 1642−51.
(20) Witan, H.; Kern, A.; Koziollek-Drechsler, I.; Wade, R.; Behl, C.; Clement, A. M. Heterodimer formation of wild-type and amyotrophic lateral sclerosis-causing mutant Cu/Zn-superoxide dismutase induces toxicity independent of protein aggregation. *Hum. Mol. Genet.* **2008**, *17* (10), 1373−85.
(21) Prudencio, M.; Durazo, A.; Whitelegge, J. P.; Borchelt, D. R. An examination of wild-type SOD1 in modulating the toxicity and aggregation of ALS-associated mutant SOD1. *Hum. Mol. Genet.* **2010**, *19* (24), 4774−89.
(22) Deng, H. X.; Shi, Y.; Furukawa, Y.; Zhai, H.; Fu, R.; Liu, E.; Gorrie, G. H.; Khan, M. S.; Hung, W. Y.; Bigio, E. H.; Lukas, T.; Dal Canto, M. C.; O'Halloran, T. V.; Siddique, T. Conversion to the amyotrophic lateral sclerosis phenotype is associated with intermolecular linked insoluble aggregates of SOD1 in mitochondria. *Proc. Natl. Acad. Sci. U.S.A.* **2006**, *103* (18), 7142−7.
(23) Xu, G.; Ayers, J. I.; Roberts, B. L.; Brown, H.; Fromholt, S.; Green, C.; Borchelt, D. R. Direct and indirect mechanisms for wild-type SOD1 to enhance the toxicity of mutant SOD1 in bigenic transgenic mice. *Hum. Mol. Genet.* **2015**, *24* (4), 1019−35.
(24) Dashnaw, C. M.; Zhang, A. Y.; Gonzalez, M.; Koone, J. C.; Shaw, B. F. Metal migration and subunit swapping in ALS-linked SOD1: Zn(2+) transfer between mutant and wild-type occurs faster than the rate of heterodimerization. *J. Biol. Chem.* **2022**, *298* (12), 102610.
(25) Shaw, B. F.; Durazo, A.; Nersissian, A. M.; Whitelegge, J. P.; Faull, K. F.; Valentine, J. S. Local unfolding in a destabilized, pathogenic variant of superoxide dismutase 1 observed with H/D exchange and mass spectrometry. *J. Biol. Chem.* **2006**, *281* (26), 18167−76.
(26) Wells, N. G. M.; Tillinghast, G. A.; O'Neil, A. L.; Smith, C. A. Free energy calculations of ALS-causing SOD1 mutants reveal common perturbations to stability and dynamics along the maturation pathway. *Protein Sci.* **2021**, *30* (9), 1804−1817.
(27) Banks, C. J.; Andersen, J. L. Mechanisms of SOD1 regulation by post-translational modifications. *Redox BIol.* **2019**, *26*, 101270.
(28) Redler, R. L.; Wilcox, K. C.; Proctor, E. A.; Fee, L.; Caplow, M.; Dokholyan, N. V. Glutathionylation at Cys-111 induces dissociation of wild type and FALS mutant SOD1 dimers. *Biochem.* **2011**, *50* (32), 7057−66.
(29) Banks, C. J.; Rodriguez, N. W.; Gashler, K. R.; Pandya, R. R.; Mortenson, J. B.; Whited, M. D.; Soderblom, E. J.; Thompson, J. W.; Moseley, M. A.; Reddi, A. R.; Tessem, J. S.; Torres, M. P.; Bikman, B. T.; Andersen, J. L. Acylation of Superoxide Dismutase 1 (SOD1) at K122 Governs SOD1-Mediated Inhibition of Mitochondrial Respiration. *Mol. Cell. Biol.* **2017**, *37* (20), e00354-17.
(30) Choudhary, C.; Kumar, C.; Gnad, F.; Nielsen, M. L.; Rehman, M.; Walther, T. C.; Olsen, J. V.; Mann, M. Lysine acetylation targets protein complexes and co-regulates major cellular functions. *Science* **2009**, *325* (5942), 834−40.
(31) Shi, Y.; Rhodes, N. R.; Abdolvahabi, A.; Kohn, T.; Cook, N. P.; Marti, A. A.; Shaw, B. F. Deamidation of asparagine to aspartate destabilizes Cu, Zn superoxide dismutase, accelerates fibrillization, and mirrors ALS-linked mutations. *J. Am. Chem. Soc.* **2013**, *135* (42), 15897−908.
(32) Uchida, K.; Kawakishi, S. Identification of oxidized histidine generated at the active site of Cu,Zn-superoxide dismutase exposed to H2O2. Selective generation of 2-oxo-histidine at the histidine 118. *J. Biol. Chem.* **1994**, *269* (4), 2405−10.
(33) Taylor, D. M.; Gibbs, B. F.; Kabashi, E.; Minotti, S.; Durham, H. D.; Agar, J. N. Tryptophan 32 potentiates aggregation and cytotoxicity of a copper/zinc superoxide dismutase mutant associated with familial amyotrophic lateral sclerosis. *J. Biol. Chem.* **2007**, *282* (22), 16329−35.
(34) Fujiwara, N.; Nakano, M.; Kato, S.; Yoshihara, D.; Ookawara, T.; Eguchi, H.; Taniguchi, N.; Suzuki, K. Oxidative modification to cysteine sulfonic acid of Cys111 in human copper-zinc superoxide dismutase. *J. Biol. Chem.* **2007**, *282* (49), 35933−44.
(35) Bosco, D. A.; Morfini, G.; Karabacak, N. M.; Song, Y.; Gros-Louis, F.; Pasinelli, P.; Goolsby, H.; Fontaine, B. A.; Lemay, N.; McKenna-Yasek, D.; Frosch, M. P.; Agar, J. N.; Julien, J. P.; Brady, S. T.; Brown, R. H., Jr. Wild-type and mutant SOD1 share an aberrant

conformation and a common pathogenic pathway in ALS. *Nat. Neurosci.* **2010**, *13* (11), 1396−403.
(36) Tsang, C. K.; Chen, M.; Cheng, X.; Qi, Y.; Chen, Y.; Das, I.; Li, X.; Vallat, B.; Fu, L. W.; Qian, C. N.; Wang, H. Y.; White, E.; Burley, S. K.; Zheng, X. F. S. SOD1 Phosphorylation by mTORC1 Couples Nutrient Sensing and Redox Regulation. *Mol. Cell* **2018**, *70* (3), 502−515.
(37) Antinone, S. E.; Ghadge, G. D.; Lam, T. T.; Wang, L.; Roos, R. P.; Green, W. N. Palmitoylation of superoxide dismutase 1 (SOD1) is increased for familial amyotrophic lateral sclerosis-linked SOD1 mutants. *J. Biol. Chem.* **2013**, *288* (30), 21606−17.
(38) Lennicke, C.; Cocheme, H. M. Redox metabolism: ROS as specific molecular regulators of cell signaling and function. *Mol. Cell* **2021**, *81* (18), 3691−3707.
(39) Poole, L. B.; Nelson, K. J. Discovering mechanisms of signaling-mediated cysteine oxidation. *Curr. Opin. Chem. Biol.* **2008**, *12* (1), 18−24.
(40) Donnelly, D. P.; Dowgiallo, M. G.; Salisbury, J. P.; Aluri, K. C.; Iyengar, S.; Chaudhari, M.; Mathew, M.; Miele, I.; Auclair, J. R.; Lopez, S. A.; Manetsch, R.; Agar, J. N. Cyclic Thiosulfinates and Cyclic Disulfides Selectively Cross-Link Thiols While Avoiding Modification of Lone Thiols. *J. Am. Chem. Soc.* **2018**, *140* (24), 7377−7380.
(41) Hossain, M. A.; Sarin, R.; Donnelly, D. P.; Miller, B. C.; Salisbury, J. P.; Conway, J. B.; Watson, S.; Winters, J. N.; Alam, N.; Sivasankar, D.; Ponmudiyan, A. C.; Gawde, T.; Kannapadi, S.; Auclair, J. R.; Makowski, L.; Petsko, G. A.; Ringe, D.; Greenblatt, D. J.; Ondrechen, M. J.; Chen, Y.; Manetsch, R.; Agar, J. N., Protein crosslinking as a therapeutic strategy for SOD1-related ALS. *bioRxiv*, in press, **2021**.
(42) Briggs, R. G.; Fee, J. A. Sulfhydryl Reactivity of Human Erythrocyte Superoxide-Dismutase - Origin of Unusual Spectral Properties of Protein When Prepared by a Procedure Utilizing Chloroform and Ethanol for Precipitation of Hemoglobin. *Biochim. Biophys. Acta* **1978**, *537* (1), 100−109.
(43) Rudyk, O.; Eaton, P. Biochemical methods for monitoring protein thiol redox states in biological systems. *Redox BIol.* **2014**, *2*, 803−813.
(44) Claiborne, A.; Mallett, T. C.; Yeh, J. I.; Luba, J.; Parsonage, D. Structural, redox, and mechanistic parameters for cysteine-sulfenic acid function in catalysis and regulation. *Advances in Protein Chemistry*; Elsevier, 2001; Vol. *58*, pp 215−276.
(45) Forman, H. J.; Ursini, F.; Maiorino, M. An overview of mechanisms of redox signaling. *J. Mol. Cell. Cardiol.* **2014**, *73*, 2−9.
(46) Paulsen, C. E.; Carroll, K. S. Orchestrating Redox Signaling Networks through Regulatory Cysteine Switches. *Acs Chem. Biol.* **2010**, *5* (1), 47−62.
(47) Lee, Y. M.; He, W. F.; Liou, Y. C. The redox language in neurodegenerative diseases: oxidative post-translational modifications by hydrogen peroxide. *Cell Death Dis.* **2021**, *12* (1), 58.
(48) van der Reest, J.; Lilla, S.; Zheng, L.; Zanivan, S.; Gottlieb, E. Proteome-wide analysis of cysteine oxidation reveals metabolic sensitivity to redox stress. *Nat. Commun.* **2018**, *9* (1), 1581.
(49) Cardey, B.; Enescu, M. Selenocysteine versus cysteine reactivity: a theoretical study of their oxidation by hydrogen peroxide. *J. Phys. Chem. A* **2007**, *111* (4), 673−8.
(50) Valle, C.; Carri, M. T. Cysteine Modifications in the Pathogenesis of ALS. *Front. Mol. Neurosci.* **2017**, *10*, 5.
(51) Xu, W. C.; Liang, J. Z.; Li, C.; He, Z. X.; Yuan, H. Y.; Huang, B. Y.; Liu, X. L.; Tang, B.; Pang, D. W.; Du, H. N.; Yang, Y.; Chen, J.; Wang, L.; Zhang, M.; Liang, Y. Pathological hydrogen peroxide triggers the fibrillization of wild-type SOD1 via sulfenic acid modification of Cys-111. *Cell Death Dis.* **2018**, *9* (2), 67.
(52) Shi, Y.; Abdolvahabi, A.; Shaw, B. F. Protein charge ladders reveal that the net charge of ALS-linked superoxide dismutase can be different in sign and magnitude from predicted values. *Protein Sci.* **2014**, *23* (10), 1417−33.
(53) Mulligan, V. K.; Kerman, A.; Laister, R. C.; Sharda, P. R.; Arslan, P. E.; Chakrabartty, A. Early steps in oxidation-induced SOD1 misfolding: implications for non-amyloid protein aggregation in familial ALS. *J. Mol. Biol.* **2012**, *421* (4−5), 631−52.
(54) Martins, D.; English, A. M. SOD1 oxidation and formation of soluble aggregates in yeast: relevance to sporadic ALS development. *Redox Biol.* **2014**, *2*, 632−9.
(55) Tiwari, M. K.; Hagglund, P. M.; Møller, I. M.; Davies, M. J.; Bjerrum, M. J. Copper ion/H2O2 oxidation of Cu/Zn-Superoxide dismutase: Implications for enzymatic activity and antioxidant action. *Redox Biol.* **2019**, *26*, 101262.
(56) Auclair, J. R.; Johnson, J. L.; Liu, Q.; Salisbury, J. P.; Rotunno, M. S.; Petsko, G. A.; Ringe, D.; Brown, R. H., Jr.; Bosco, D. A.; Agar, J. N. Post-translational modification by cysteine protects Cu/Zn-superoxide dismutase from oxidative damage. *Biochem.* **2013**, *52* (36), 6137−44.
(57) Molnar, K. S.; Karabacak, N. M.; Johnson, J. L.; Wang, Q.; Tiwari, A.; Hayward, L. J.; Coales, S. J.; Hamuro, Y.; Agar, J. N. A common property of amyotrophic lateral sclerosis-associated variants: destabilization of the copper/zinc superoxide dismutase electrostatic loop. *J. Biol. Chem.* **2009**, *284* (45), 30965−73.
(58) Shi, Y.; Mowery, R. A.; Shaw, B. F. Effect of Metal Loading and Subcellular pH on Net Charge of Superoxide Dismutase-1. *J. Mol. Biol.* **2013**, *425*, 4388.
(59) Trist, B. G.; Genoud, S.; Roudeau, S.; Rookyard, A.; Abdeen, A.; Cottam, V.; Hare, D. J.; White, M.; Altvater, J.; Fifita, J. A.; Hogan, A.; Grima, N.; Blair, I. P.; Kysenius, K.; Crouch, P. J.; Carmona, A.; Rufin, Y.; Claverol, S.; Van Malderen, S.; Falkenberg, G.; Paterson, D. J.; Smith, B.; Troakes, C.; Vance, C.; Shaw, C. E.; Al-Sarraj, S.; Cordwell, S.; Halliday, G.; Ortega, R.; Double, K. L. Altered SOD1 maturation and post-translational modification in amyotrophic lateral sclerosis spinal cord. *Brain* **2022**, *145*, 3108.
(60) Berdynski, M.; Miszta, P.; Safranow, K.; Andersen, P. M.; Morita, M.; Filipek, S.; Zekanowski, C.; Kuzma-Kozakiewicz, M. SOD1 mutations associated with amyotrophic lateral sclerosis analysis of variant severity. *Sci. Rep.* **2022**, *12* (1), 103.
(61) Gertsman, I.; Wuu, J.; McAlonis-Downes, M.; Ghassemian, M.; Ling, K.; Rigo, F.; Bennett, F.; Benatar, M.; Miller, T. M.; Da Cruz, S. An endogenous peptide marker differentiates SOD1 stability and facilitates pharmacodynamic monitoring in SOD1 amyotrophic lateral sclerosis. *JCI Insight* **2019**, *4* (10), e122768.
(62) Tokuda, E.; Takei, Y. I.; Ohara, S.; Fujiwara, N.; Hozumi, I.; Furukawa, Y. Wild-type Cu/Zn-superoxide dismutase is misfolded in cerebrospinal fluid of sporadic amyotrophic lateral sclerosis. *Mol. Neurodegener.* **2019**, *14* (1), 42.
(63) Bradshaw, R. T.; Dziedzic, J.; Skylaris, C. K.; Essex, J. W. The Role of Electrostatics in Enzymes: Do Biomolecular Force Fields Reflect Protein Electric Fields? *J. Chem. Inf. Model* **2020**, *60* (6), 3131−3144.
(64) Chen, L. X.; Xu, H. F.; Wang, P. S.; Yang, X. X.; Wu, Z. Y.; Li, H. F. SOD1Mutation Spectrum and Natural History of ALS Patients in a 15-Year Cohort in Southeastern China. *Front. Genet.* **2021**, *12*, 746060.
(65) Nakamura, A.; Hineno, A.; Yoshida, K.; Sekijima, Y.; Hanaoka-Tachibana, N.; Takei, Y.; Ohara, S.; Ikeda, S. Marked intrafamilial phenotypic variation in a family with SOD1 C111Y mutation. *Amyotroph. Lateral Scler.* **2012**, *13* (5), 479−86.
(66) Eisen, A.; Mezei, M. M.; Stewart, H. G.; Fabros, M.; Gibson, G.; Andersen, P. M. SOD1 gene mutations in ALS patients from British Columbia, Canada: clinical features, neurophysiology and ethical issues in management. *Amyotroph. Lateral Scler.* **2008**, *9* (2), 108−19.
(67) Cozzolino, M.; Amori, I.; Pesaresi, M. G.; Ferri, A.; Nencini, M.; Carri, M. T. Cysteine 111 affects aggregation and cytotoxicity of mutant Cu,Zn-superoxide dismutase associated with familial amyotrophic lateral sclerosis. *J. Biol. Chem.* **2008**, *283* (2), 866−874.
(68) Lepock, J. R.; Frey, H. E.; Hallewell, R. A. Contribution of Conformational Stability and Reversibility of Unfolding to the Increased Thermostability of Human and Bovine Superoxide-Dismutase Mutated at Free Cysteines. *J. Biol. Chem.* **1990**, *265* (35), 21612−21618.

https://doi.org/10.1021/acschemneuro.3c00174
ACS Chem. Neurosci. 2023, 14, 1547−1560

(69) Toichi, K.; Yamanaka, K.; Furukawa, Y. Disulfide Scrambling Describes the Oligomer Formation of Superoxide Dismutase (SOD1) Proteins in the Familial Form of Amyotrophic Lateral Sclerosis. *J. Biol. Chem.* **2013**, *288* (7), 4970−4980.
(70) Nagano, S.; Takahashi, Y.; Yamamoto, K.; Masutani, H.; Fujiwara, N.; Urushitani, M.; Araki, T. A cysteine residue affects the conformational state and neuronal toxicity of mutant SOD1 in mice: relevance to the pathogenesis of ALS. *Hum. Mol. Genet.* **2015**, *24* (12), 3427−39.
(71) Smith, E. F.; Shaw, P. J.; De Vos, K. J. The role of mitochondria in amyotrophic lateral sclerosis. *Neurosci. Lett.* **2019**, *710*, 132933.
(72) Verber, N.; Shaw, P. J. Biomarkers in amyotrophic lateral sclerosis: a review of new developments. *Curr. Opin. Neurol.* **2020**, *33* (5), 662−668.
(73) Waller, R.; Wyles, M.; Heath, P. R.; Kazoka, M.; Wollff, H.; Shaw, P. J.; Kirby, J. Small RNA Sequencing of Sporadic Amyotrophic Lateral Sclerosis Cerebrospinal Fluid Reveals Differentially Expressed miRNAs Related to Neural and Glial Activity. *Front. Neurosci.* **2018**, *11*, 731.
(74) Bozzo, F.; Mirra, A.; Carri, M. T. Oxidative stress and mitochondrial damage in the pathogenesis of ALS: New perspectives. *Neurosci. Lett.* **2017**, *636*, 3−8.
(75) Arakawa, Y.; Itoh, S.; Fukazawa, Y.; Ishiguchi, H.; Kohmoto, J.; Hironishi, M.; Ito, H.; Kihira, T. Association between oxidative stress and microRNA expression pattern of ALS patients in the high-incidence area of the Kii Peninsula. *Brain Res.* **2020**, *1746*, 147035.
(76) An, T.; Shi, P.; Duan, W.; Zhang, S.; Yuan, P.; Li, Z.; Wu, D.; Xu, Z.; Li, C.; Guo, Y. Oxidative stress and autophagic alteration in brainstem of SOD1-G93A mouse model of ALS. *Mol. Neurobiol.* **2014**, *49* (3), 1435−48.
(77) Bakshi, R.; Xu, Y.; Mueller, K. A.; Chen, X.; Granucci, E.; Paganoni, S.; Sadri-Vakili, G.; Schwarzschild, M. A. Urate mitigates oxidative stress and motor neuron toxicity of astrocytes derived from ALS-linked SOD1(G93A) mutant mice. *Mol. Cell. Neurosci.* **2018**, *92*, 12−16.
(78) Blasco, H.; Garcon, G.; Patin, F.; Veyrat-Durebex, C.; Boyer, J.; Devos, D.; Vourc'h, P.; Andres, C. R.; Corcia, P. Panel of Oxidative Stress and Inflammatory Biomarkers in ALS: A Pilot Study. *Can. J. Neurol. Sci.* **2017**, *44* (1), 90−95.
(79) Benkler, C.; Barhum, Y.; Ben-Zur, T.; Offen, D. Multifactorial Gene Therapy Enhancing the Glutamate Uptake System and Reducing Oxidative Stress Delays Symptom Onset and Prolongs Survival in the SOD1-G93A ALS Mouse Model. *J. Mol. Neurosci.* **2016**, *58* (1), 46−58.
(80) Barber, S. C.; Shaw, P. J. Oxidative stress in ALS: key role in motor neuron injury and therapeutic target. *Free Radic. Biol. Med.* **2010**, *48* (5), 629−41.
(81) Rasouli, S.; Abdolvahabi, A.; Croom, C. M.; Plewman, D. L.; Shi, Y.; Ayers, J. I.; Shaw, B. F. Lysine acylation in superoxide dismutase-1 electrostatically inhibits formation of fibrils with prion-like seeding. *J. Biol. Chem.* **2017**, *292* (47), 19366−19380.
(82) Cieplak, P.; Cornell, W. D.; Bayly, C.; Kollman, P. A. *J. Comput. Chem.* **1995**, *16*, 1357.
(83) Roe, D. R.; Cheatham, T. E., III *J. Chem. Theory Comput.* **2013**, *9*, 3084.
(84) Case, D. A.; Cheatham, T. E., III; Darden, T.; Gohlke, H.; Luo, R.; Merz Jr, K. M.; Onufriev, A.; Simmerling, C.; Wang, B.; Woods, R. J. *J. Comput. Chem.* **2005**, *26*, 1668.
(85) Case, D. A.; Belfon, K.; Ben-Shalom, I. Y.; Brozell, S. R.; Cerutti, D. S.; Cheatham, T. E., III; Cruzeiro, V. W. D.; Darden, T. A.; Duke, R. E.; Giambasu, G.; Gilson, M. K.; Gohlke, H.; Goetz, A. W.; Harris, R.; Izadi, S.; Izmailov, S. A.; Kasavajhala, K.; Kovalenko, A.; Krasny, R.; Kurtzman, T.; Lee, T. S.; LeGrand, S.; Li, P.; Lin, C.; Liu, J.; Luchko, T.; Luo, R.; Man, V.; Merz, K. M.; Miao, Y.; Mikhailovskii, O.; Monard, G.; Nguyen, H.; Onufriev, A.; Pan, F.; Pantano, S.; Qi, R.; Roe, D. R.; Roitberg, A.; Sagui, C.; Schott-Verdugo, S.; Shen, J.; Simmerling, C. L.; Skrynnikov, N. R.; Smith, J.; Swails, J.; Walker, R. C.; Wang, J.; Wilson, L.; Wolf, R. M.; Wu, X.; Xiong, Y.; Xue, Y.; York, D. M.; Kollman, P. A. *AMBER 2020*; University of California: San Francisco, CA, 2020.
(86) Keith, T. A.; Millam, J. M. *Gauss View*, Version 6; Semichem Inc., 2016.
(87) Frisch, M.; Trucks, G.; Schlegel, H.; Scuseria, G.; Robb, M.; Cheeseman, J.; Scalmani, G.; Barone, V.; Petersson, G.; Nakatsuji, H.; et al. *Gaussian 16*; Gaussian Inc.: Wallingford CT, 2016.
(88) Singh, U. C.; Kollman, P. A. *Journal of computational chemistry* **1984**, *5*, 129.
(89) Besler, B. H.; Merz, K. M., Jr.; Kollman, P. A. *J. Comput. Chem.* **1990**, *11*, 431.
(90) Hornak, V.; Abel, R.; Okur, A.; Strockbine, B.; Roitberg, A.; Simmerling, C. *Proteins* **2006**, *65*, 712.
(91) Strange, R. W.; Antonyuk, S. V.; Hough, M. A.; Doucette, P. A.; Valentine, J. S.; Hasnain, S. S. *J. Mol. Biol.* **2006**, *356*, 1152.
(92) Anandakrishnan, R.; Aguilar, B.; Onufriev, A. V. *Nucleic Acids Res.* **2012**, *40*, W537.
(93) Myers, J.; Grothaus, G.; Narayanan, S.; Onufriev, A. *Proteins: Struct. Funct. Genet.* **2006**, *63*, 928.
(94) Gordon, J. C.; Myers, J. B.; Folta, T.; Shoja, V.; Heath, L. S.; Onufriev, A. *Nucleic Acids Res.* **2005**, *33*, W368.
(95) Humphrey, W.; Dalke, A.; Schulten, K. *J. Mol. Graphics* **1996**, *14*, 33.
(96) Jorgensen, W. L.; Chandrasekhar, J.; Madura, J. D.; Impey, R. W.; Klein, M. L. *J. Chem. Phys.* **1983**, *79*, 926.
(97) Joung, I. S.; Cheatham, T. E., III *J. Phys. Chem. B* **2008**, *112*, 9020.
(98) Darden, T.; York, D.; Pedersen, L. *J. Chem. Phys.* **1993**, *98*, 10089.
(99) Ryckaert, J.-P.; Ciccotti, G.; Berendsen, H. J. *J. Comput. Phys.* **1977**, *23*, 327.
(100) Miyamoto, S.; Kollman, P. A. *J. Comput. Chem.* **1992**, *13*, 952.
(101) Gotz, A. W.; Williamson, M. J.; Xu, D.; Poole, D.; Le Grand, S.; Walker, R. C. *J. Chem. Theory Comput.* **2012**, *8*, 1542.

https://doi.org/10.1021/acschemneuro.3c00174
ACS Chem. Neurosci. 2023, 14, 1547−1560